Article

Reduction- and pH-sensitive Hyaluronan Nanoparticles for Delivery of Iridium(III) Anticancer Drugs

Zhixiang Cai, Hongbin Zhang, Yue Wei, Yuanyuan Wei, Yanping Xie, and Fengsong Cong

Biomacromolecules, **Just Accepted Manuscript** • Publication Date (Web): 12 Jun 2017

Reduction- and pH-sensitive Hyaluronan Nanoparticles for Delivery of Iridium(III) Anticancer Drugs

Zhixiang Cai[†], *Hongbin Zhang*[†]*, *Yue Wei*[†], *Yuanyuan Wei*[†], *Yanping Xie*[†], *Fengsong Cong*[††]

[†]Department of Polymer Science and Engineering, School of Chemistry and Chemical Engineering, Shanghai Jiao Tong University, Shanghai, 200240, China

[††]Department of Biochemistry and Molecular Biology, School of life Sciences and Biotechnology, Shanghai Jiao Tong University, Shanghai 200240, China

E-mail: hbzhang@sjtu.edu.cn

KEYWORDS: Hyaluronic acid; glycosaminoglycan; organoiridium complex; nanoparticles; drug delivery; targeted anticancer efficacy

ABSTRACT: The organoiridium(III) complex (Ir(III)) [(η^5-Cp^{xbiph})Ir(phpy)(py)]PF_6 containing π-bonded biphenyltetramethylcyclopentadienyl(Cpxbiph), C^N-chelated phenylpyridine(phpy), and pyridine (py) ligands has more potent antitumor activity as a new generation of drug than cisplatin toward various cancer cells. However, poor site-specific delivery, low solubility, and poor tumor penetration are common limitations of chemotherapy drugs. To develop CD44-targetable, pH-, and reduction-responsive drug delivery systems for Ir(III) drugs, the amphiphilic hyaluronan (HA)-based conjugates of HA-cystamin-pyrenyl (HA-ss-Py) containing disulfide

bonds and HA-pyrenyl (HA-Py) were designed. The Ir(III) drug was readily loaded into these two amphiphilic conjugates and nanoparticles were formed. Dynamic light scattering (DLS) studies showed that the micelles formed from HA-ss-Py were sufficiently stable under physiological conditions, but were prone to rapid dissociation in reducing environments (20 mM glutathione (GSH)). In subsequent confocal microscopy analyses, A549 cancer cells efficiently internalized HA-based micelles. Moreover, in vitro cytotoxicity assays in A549 cells demonstrat that Ir-loaded HA-based nanoparticles have higher cytotoxicity than the free Ir(III) anticancer drug. Finally, systemic administration of Ir(III)-loaded HA-ss-Py nanoparticles enhanced tumor inhibition *in vivo*, and the corresponding biodistribution experiments showed that HA-ss-Py micelles accumulate in tumors. Overall, our results suggest that HA-ss-Py micelles have a great potential to be used as an effective Ir(III) drug carrier for targeted cancer therapy.

INTRODUCTION

Platinum-based anticancer drugs such as cisplatin, carboplatin, and oxaliplatin have received global approval.[1, 2] However, most of these drugs suffer from insolubility in water and platinum resistance, and they cause several undesirable side effects, including nephrotoxicity and neurotoxicity. These properties limit the future use of these preparations, despite their current wide application to the treatment of most cancers.[3, 4] With these challenges in mind, considerable efforts have been made to develop alternative organometallic complexes of platinum-group metals, such as ruthenium, osmium, rhodium, and iridium, with reduced side effects and an efficacy against a wider range of cancers.[5-8] In particular, organoiridium(III) complexes (Ir(III)) show promising anticancer activities,[9-11] and half-sandwich cyclopentadienyl iridium(III) complexes with potent anticancer activity are also well suited for development as anticancer agents.[12-16] A new generation of anticancer drugs comprising the Ir(III) [(η^5-

Cp^{xbiph})Ir(phpy)(py)]PF_6, containing π-bonded biphenyltetramethylcyclopentadienyl (Cp^{xbiph}), C^N-chelated phenylpyridine (phpy), and pyridine (py) ligands, had potent antitumor activity in a previous study, reflecting potent stimulation of reactive oxygen species production.[13]

Chemotherapy is the most common treatment for several solid tumor malignancies.[17] However, the ensuing therapeutic effects remain suboptimal, mostly due to poor solubility and bioavailability, nonspecific selectivity.[18, 19] To address these limitations of chemotherapeutic agents, many drug delivery approaches have been investigated with the intention of transporting drugs to tumor targets without damaging healthy tissues and organs. Medical applications of nanotechnology (nanomedicine) have stimulated the development of various types of drug-loaded nanocarriers, such as liposomes,[20-22] carbon nanomaterials,[23, 24] inorganic materials,[25, 26] and polymeric particulates.[27, 28] In particular, self-assembled nanoparticles have received an increasing interest as promising nanocarriers that encapsulate and mediate the sustained release of various hydrophobic anticancer drugs.[29, 30] Drugs can be entrapped in interior structures or adsorbed to exterior surfaces of nanoparticles, and most nanoparticles have multiple advantages over their small molecule counterparts, including improved thermodynamic stability, prolonged circulation times, reduced systemic toxicity, and improved passive accumulation in cancer cells due to enhanced permeability and retention (EPR) effects.[31-34] Hence, due to the potential applications of these properties to cancer chemotherapies, various synthetic and natural materials have recently been developed as nanocarriers for cancer treatment.[35, 36] In particular, polysaccharides have promising biocompatibility, biodegradability, hydrophilicity, and ease of chemical modification, and have been widely used as building blocks for the construction of nanoparticle drug delivery systems.[37]

Despite the advantages of nanoparticles, clinical trials of drug-loaded, self-assembled nanoparticles continue to face technical challenges such as poor stability in the bloodstream following intravenous injections, and undesirable premature drug release at unwanted sites, resulting in a lower therapeutic efficacy.[38] Therefore, drug delivery systems with structures that respond to external stimuli (including reduction, light, pH, and enzyme activities) are ideal candidates for the controlled release of anticancer drugs.[39-42] Hence, drug nanocarriers that are responsive to pH and reducing environments have received tremendous attention as extra- and intra-cellular environments differ strongly in pH and reduction potential.[43] Specifically, it is well known that the natural disulfide bond-reducing agent glutathione (GSH) is present at higher concentrations in the cytoplasm than in the plasma.[44] Hence, nanoparticles with characteristic disulfide linkages offer an attractive strategy for drug delivery systems, because although nanoparticles are sufficiently stable under physiological conditions and in blood, rapid reduction of disulfide bonds leads to the dissociation of nanoparticles inside the cells with high GSH concentrations.[45, 46] In addition, the pH of tumor tissues is lower than that of blood and normal tissue, while endosomes and lysosomes have even lower pH values of 5.0-5.5.[47, 48] Accordingly, the pH- and reduction-responsive drug delivery systems have recently received increasing attention.[49-52]

Despite the promise of drug release responses to external stimuli, practical nanocarriers need to specifically target cancer cells. Hyaluronan or hyaluronic acid (HA) is a naturally occurring linear polysaccharide comprising alternating repeat units of D-glucuronic acid and N-acetyl glycosamine linked by β-(1,4) and β-(1,3) glycosidic bonds.[53] HA has been extensively used in biomedical and pharmaceutical fields because of its desirable physiochemical properties, including biodegradability, cytocompatibility, nonimmunogenicity, and high water-binding

capacity. In addition, HA has a uniquely high affinity for the CD44 receptor binding.[54-57] Previous studies have investigated the use of HA as a delivery vehicle in many drug-delivery systems, reflecting its interactions with multiple cancer cell types that present abundant HA receptors (CD44 and RHAMM).[53, 58, 59] Several studies report the use of HA and its derivatives as nanoparticles for cancer imaging and therapy, and in comparison with free anticancer drugs, these HA nanocarriers have enhanced tumor targeting abilities and therapeutic efficacy, and provide strategies for controlled drug release.[60-64]

In the present study, we developed novel amphiphilic micelles comprising disulfide cross-linked HA-cystamine-pyrenyl conjugates (HA-ss-Py) for facile loading (Scheme 1A) and CD44-targeted therapy, in conjunction with pH- and reduction-triggered intracellular release of Ir(III) anticancer drugs (Scheme 1B). The tumor inhibition efficacy of Ir-loaded HA-ss-Py nanoparticles was compared with that of Ir-loaded HA-pyrenyl (HA-Py) nanoparticles and free Ir anticancer drugs in tumor-bearing mice.

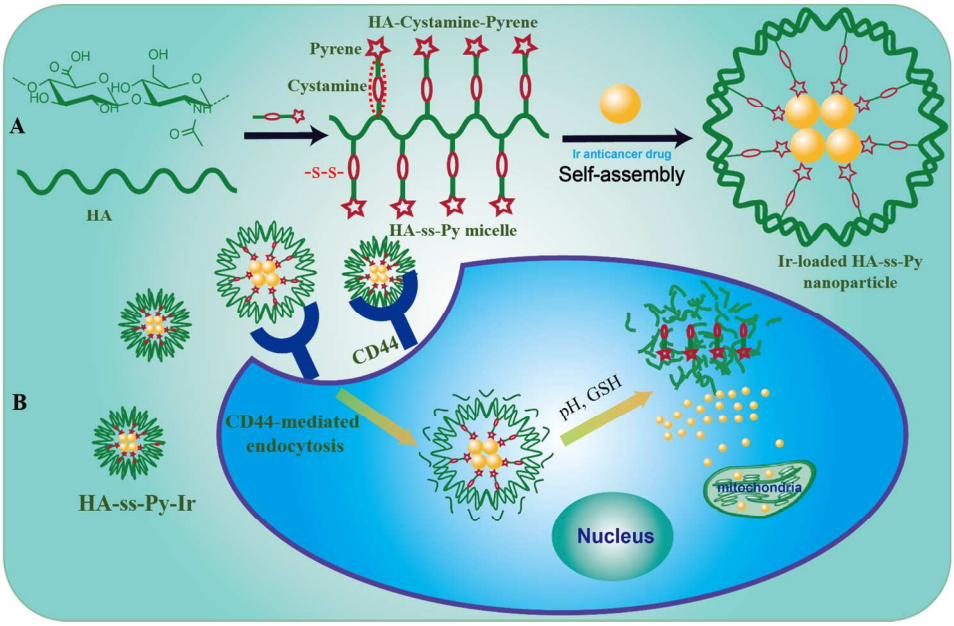

Scheme 1 Illustration of HA-based micelles as multifunctional platform for the active CD44-targeting Ir anticancer drug delivery. (A) Formation of self-assembled nanoparticles comprising disulfide cross-linked HA-cystamin-pyrenyl conjugates (HA-ss-Py) for facile loading Ir(III) anticancer, (B) CD44-mediated uptake of nanoparticles and dual-triggered (pH- and reduction) intracellular release of Ir(III) anticancer drugs, which triggers apoptosis in cancer cells.

EXPERMENTAL SECTION

Materials

Sodium hyaluronan (HA, M_w = 10kDa) was purchased from Shandong Freda Biopharm Co., Ltd, and 4-bromo-biphenyl, 2,3,4,5-tetramethyl-2-cyclopentenone (95%), tert-butyllithium solution (1.3 M in hexane), $IrCl_3 \cdot nH_2O$, 2-phenylpyridine, ammonium hexafluorophosphate, silver nitrate, 1-ethyl-3-(3-dimethylaminopropyl) carbodiimide (EDC), N-hydroxysuccinimide (NHS), 1-Hydroxybenzotriazole (HOBt), pyrene, cystamine, glutathione (GSH), 1,4-diaminobutane, 1-pyrenebutyric acid, Dimethyl Sulphoxide (DMSO) and formamide were purchased from Sigma-Aldrich. The near-infrared dye Cy5.5 (99%) was purchased from Shanghai Seebio Biotech Inc. Nile red and Hoechst 33342 were obtained from Aladdin (Shanghai, China), and 3-(4,5-dimethyl-thiazol-2-yl)-2,5-diphenyl tetrazolium bromide (MTT), RPMI-1640 medium, penicillin, streptomycin, fetal bovine serum (FBS) trypsin/EDTA, phosphate-buffered saline (PBS), and 4% paraformaldehyde were purchased from Shanghai Ruian Biotechnology Co., Ltd. The A549 cell line was obtained from the Chinese academy of science. Dialysis membranes (MWCO, 3500 Da) were purchased from Spectrum Laboratories (Rancho Dominguez, CA, USA). All other reagents and chemicals were of analytical grade and

were used without further purification. All aqueous solutions were prepared using ultrapure water (> 18 MU) from a Milli-Q Plus system (Millipore).

Synthesis of Ir(III) anticancer drugs

Synthesis of compound 1 tetramethyl-(biphenyl)cyclopentadienyl ($Cp^{xbiph}H$)

$Cp^{xbiph}H$ was synthesized according to a previously reported protocol with some adaptations.[65] Briefly, 4-bromo-biphenyl (4.66 g, 20 mmol) was dissolved in anhydrous tetrahydrofuran (THF, 80 mL) with stirring, until a clear solution was obtained. Tert-butyllithium solution (1.3 M in hexane, 12.5 mL, 20 mmol) was then added slowly to an oven-dried three-necked flask containing the above-mentioned solution under N_2 atmosphere at 195 K, and the mixture was stirred at this temperature for 3 h. Subsequently, 2,3,4,5-tetramethyl-2-cyclopentenone (3.32 g, 24 mmol) was added dropwise into the reaction mixture and was then warmed slowly to room temperature with stirring overnight. After completion (monitored by TLC), HCl (36%, 10 mL) was added to the orange solution. The mixture was then extracted with diethyl ether (30 mL × 2) and the combined organic layers were dried using $MgSO_4$, filtered, and were finally concentrated *in vacuo*. The residue was recrystallized from chloroform and hexane (3:1) to produce the desired product as a yellow powder. All yields were obtained after recrystallization. Yield: 1.86 g (34%), ^{1}H-NMR ($CDCl_3$): δ = 7.68 (m, 4H), 7.46 (m, 2H), 7.35 (m, 3H), 3.27 (m, 1H), 2.12 (s, 3H), 1.98 (s, 3H), 1.92 (s, 3H), 1.02 (d, 3H, J = 8.0Hz).

Synthesis of compound 2 $[(\eta^5\text{-}Cp^{xbiph})IrCl_2]_2$

The compound $[(\eta^5\text{-}Cp^{xbiph})IrCl_2]_2$ was prepared as reported previously with the protocol modifications described below.[65] Briefly, $Cp^{xbiph}H$ (1.37 g, 5 mmol) and $IrCl_3 \cdot nH_2O$ (1.19 g,

4mmol) were added to 60 mL of anhydrous methanol. The suspension was then refluxed under vigorous stirring for 48 h in a N_2 atmosphere. After completion of the reaction, the reaction mixture was cooled to room temperature and the resulting orange precipitate was filtered and thoroughly washed with anhydrous methanol (20 mL × 2) and diethyl ether (20 mL × 2), and was finally dried under vacuum at 323 K to produce the desired product. Yield: 1.15 g (43.4%), ^{1}H-NMR (DMSO-d_6): δ = 7.70 (m, 6H), 7.42 (m, 2H), 7.39 (m, 1H), 1.73 (d, 12H, J = 8.0 Hz).

Synthesis of compound 3 [(η^5-Cp^{xbiph})Ir(phpy)Cl]

The compound [(η^5-Cp^{xbiph})Ir(phpy)Cl] was prepared as described in a previous report.[11] Briefly, [(η^5-Cp^{xbiph})IrCl$_2$]$_2$ (1.06 g, 1 mmol), 2-phenylpyridine (0.36 g, 2.4 mmol), and sodium acetate (0.32 g, 4 mmol) were added to anhydrous CH_2Cl_2 (20 mL) and the mixture was refluxed in a N_2 atmosphere for 24 h and was then filtered. The filtrate was then evaporated and the powder was recrystallized from $CHCl_3$/hexane (3:1) to produce the desired product. Yield: 0.66 g (50%), ^{1}H-NMR ($CDCl_3$): δ = 8.53 (d, 1H, J = 4.0Hz), 7.85 (d, 1H, J = 8.0 Hz), 7.74 (m, 2H), 7.64 (m, 5H), 7.51 (m, 4H), 7.39 (d, 1H, J = 8.0 Hz), 7.19 (t, 1H, J = 8.0 Hz), 7.08 (t, 1H, J = 8.0 Hz), 6.96 (t, 1H, J = 8.0 Hz), 1.85 (s, 3H), 1.82 (s, 3H), 1.80 (s, 3H), 1.62 (s, 3H).

Synthesis of compound 4 [(η^5-Cp^{xbiph})Ir(phpy)(py)]PF$_6$

The compound [(η^5-Cp^{xbiph})Ir(phpy)(py)]PF$_6$ was synthesized using a published procedure with slight modifications.[13] Briefly, [(η^5- Cp^{xbiph})Ir(phpy)Cl] (0.33 g, 0.5 mmol) and $AgNO_3$ (0.09 g, 0.5 mmol) were successively added to anhydrous MeOH (10 mL) and stirred under reflux in a N_2 atmosphere for 10 h. The precipitate was filtered and pyridine (0.16 g, 2 mmol) was added with gentle stirring for 12 h. NH_4PF_6 (0.33g, 2mmol) was then added and the resulting yellow precipitate was collected by filtration. Purification of the crude product provided

the desired product following recrystallization in methanol/diethyl (1:1). Yield: 0.21 g (25%), ^{1}H-NMR ($CDCl_3$): δ = 9.00 (d, 1H, *J* = 8.0 Hz), 8.54 (d, 2H, *J* = 8.0 Hz), 7.81 (m, 3H), 7.70 (t, 2H, *J* = 8.0Hz), 7.57 (d, 2H, *J* = 8.0 Hz), 7.45(m, 5H), 7.33 (m, 4H), 7.23 (t, 1H, *J* = 8.0 Hz), 6.93 (d, 2H, *J* = 8.0 Hz), 1.90 (s, 3H), 1.82 (s, 3H), 1.66 (s, 3H), 1.61 (s, 3H).

Synthesis and characterization of Hyaluronan-Diaminobutane-Pyrene (HA-Py) and Hyaluronan-Cystamine-Pyrene (HA-ss-Py) conjugates

Synthesis and characterization of diaminobutane- and cystamine-modified HA

Diaminobutane- and cystamine-modified HA were synthesized using well-established carbodiimide chemistry. Specifically, 10 mg/mL HA (Mw, 10 kDa, 1 g) in ultrapure water (100 mL) was activated in the presence of EDC (0.96 g, 5 mmol) and HOBt (0.68 g, 5 mmol) with stirring for 30 min at room temperature. Subsequently, 1,4-diaminobutane (0.44 g, 5 mmol) was added dropwise into the solution using a pipette. The mixture was stirred at room temperature for 24 h and was then dialyzed (MWCO, 3500) against deionized water for 3 days. Finally, the HA-diaminobutane conjugate was obtained as a white powder by lyophilization. Cystamine-modified HA was prepared as described below. In a typical experiment, EDC (0.96 g, 5 mmol) and HOBt (0.68 g, 5 mmol) were slowly added to the HA solution (100 mL, 10 mg/mL) with vigorous stirring for 20 min. Cystamine dihydrochloride (0.57g, 5mmol) was then added and the reaction was allowed to proceed for 24 h at room temperature. Subsequently, the reaction mixture was dialyzed for 3 days against ultrapure water and was freeze-dried to obtain white floccules. These products were stored at 4^{o}C until further use. The chemical structures of HA-diaminobutane and HA-ss were characterized using FT-IR and ^{1}H-NMR (400 MHz). Ratios of diaminobutane and cystamine to HA were determined using ^{1}H-NMR analysis after dissolution in D_2O. ^{1}H-NMR

analyses were performed using an AVANCE III 400 spectrometer (Bruker Co., Switzerland). FT-IR spectra were recorded using a Perkin-Elmer Spectrum 100 FT-IR spectrometer (Perkin Elmer Co., USA) in the range from 4000 to 400 cm^{-1} according to the KBr sample holder method.

Synthesis and characterization of amphiphilic HA-Py and HA-ss-Py conjugates

HA-Py and HA-ss-Py were prepared by amidation of the carboxyl groups of 1-pyrenebutyric acid with the amine groups of HA-diaminobutane and HA-ss, respectively. Briefly, to activate carboxyl groups, 1-pyrenebutyric acid (0.06 g, 0.2 mmol) was added to DMSO (15 mL) in the presence of EDC (0.04 g, 0.2 mmol) and NHS (0.02 g, 0.2 mmol) with stirring for 1 h at room temperature. HA-diaminobutane (0.28 g) and HA-ss (0.28 g) conjugates were then dissolved in 20 mL of formamide, and 1-pyrenebutyric acid in DMSO was added dropwise. Reaction mixtures were incubated for 24 h at room temperature with vigorous stirring and were then dialyzed against excess ultrapure water for 3 days (MWCO, 3500 Da). Finally, suspensions were lyophilized to obtain HA-Py and HA-ss-Py conjugates. The products were stored at $4^{o}C$ for further use. The chemical structures of HA-Py and HA-ss-Py conjugates were determined using ^{1}H-NMR and FT-IR analysis. Ratios of 1-pyrenebutyric acid were determined using ^{1}H-NMR in D_2O/d_6-DMSO co-solvent (1:1 volume ratio).

Preparation and Characterization of HA-Py and HA-ss-Py micelles

HA-Py and HA-ss-Py micelles were prepared as described below. Briefly, HA-Py conjugates (15 mg) were dispersed in ultrapure water (5 mL) and the solutions were ultrasonicated for 30 min at 100 W with an ultrasonication probe. Conjugates were then filtered

through a 0.45 μm membrane filter and were lyophilized. HA-ss-Py micelles were prepared under the same conditions.

Critical micelle concentrations (CMC) of HA-Py and HA-ss-Py were determined using fluorescence spectrophotometry with pyrene as fluorescence probe. Briefly, a 10^{-6} M pyrene solution was prepared in acetone, and 1 mL aliquots were transferred into a series of 10 mL volumetric flasks and the acetone was evaporated for 5 h at room temperature. HA-Py or HA-ss-Py solutions with concentrations ranging from 10^{-5} to 0.1 mg/mL were added to volumetric flasks and were stirred for 2 h at room temperature. Fluorescence intensity was recorded using a fluorescence spectrophotometer and emissions at 374 and 385 nm were determined following excitation at 330 nm. CMC were estimated as intensity ratios of I_{374}/I_{385} at low and high concentrations.

Particle sizes and zeta potentials of HA-Py and HA-ss-Py micelles in PBS at pH=7.4 and 5.0, respectively, were detected using dynamic light scattering (DLS) (Nano-ZS90, Malvern instruments, UK). All measurements were performed at a constant temperature of 25°C and at an angle of 90°. Micelles were filtered through 0.45 μm membrane filters before measurements, and morphological characteristics of HA-Py and HA-ss-Py micelles were observed using transmission electron microscope (TEM) with a JEM-2100F apparatus operated at 200 kV. Atomic force microscope (AFM) analyses were performed using a Nano Scope IIIa (Veeco, USA) instrument and images were recorded.

pH- and reduction-triggered disassembly of micelles

Changes in the sizes and size distributions of HA-ss-Py micelles were monitored using DLS measurements after incubation in PBS buffer (pH=7.4, 0.1 M) containing GSH at 2 μM, 10 mM,

and 20 mM. Disassembly of HA-ss-Py micelles at different pH values was also characterized using DLS after incubation in PBS buffer (pH=7.4, and 5.0, respectively). HA-Py micelles were used as a reduction-insensitive control. In a typical experiment, HA-Py and HA-ss-Py micelles were prepared as above and GSH solutions of specified concentrations were added and stirred at room temperature in volumetric flasks containing reduction-sensitive HA-ss-Py micellar suspensions (0.2 mg/mL). Size distribution of HA-ss-Py micelles were recorded at various time intervals using DLS measurements. HA-Py micelles were used as a reduction-insensitive control.

Encapsulation of Ir(III) anticancer drugs

Ir(III) loaded HA-Py (HA-Py-Ir) and HA-ss-Py (HA-ss-Py-Ir) were prepared using dialysis methods. Briefly, 15 mg samples of HA-Py or HA-ss-Py were added dropwise to 3 mL of ultrapure water with stirring for 30 min at room temperature to enable complete stabilization. Subsequently, 10 mg of Ir(III) in DMSO (3 mL) was added to the suspension with stirring at room temperature for 1 h and dialysis against excess amounts of ultrapure water was performed using dialysis membranes (MWCO, 3500 Da) at room temperature for 3 days. Dispersions were filtered through 0.45 μm pore membranes to remove the unloaded Ir, and were then lyophilized to obtain a yellow powder.

Morphological characteristics of Ir(III)-loaded nanoparticles were observed using TEM and AFM, and sizes distribution of Ir(III)-loaded nanoparticles at pH 5.0 or pH 7.4 with and without GSH were characterized using DLS.

Ir loading contents (LE) and encapsulation efficiencies (EE) of Ir anticancer complexes were determined using UV-Vis spectrophotometry following dispersion of Ir-loaded micelles (HA-Py-Ir and HA-ss-Py-Ir) in ethanol/water (1:1 v/v). A calibration curve was generated from a series of

Ir solutions (ethanol: water =1:1) with varying Ir concentrations. LE and EE were calculated as follows:

$$\text{Loading content (wt\%)} = \frac{\text{weight of loaded drug in formulation}}{\text{weight of polymer in formulation}} \times 100\% \quad (1)$$

$$\text{Loading efficiency (\%)} = \frac{\text{weight of loaded drug in formulation}}{\text{weight of drug in feed}} \times 100\% \quad (2)$$

***In vitro* Release of Ir-loaded nanoparticles**

The drug release profiles of HA-Py-Ir and HA-ss-Py-Ir nanoparticles were investigated using dialysis techniques. Lyophilized HA-Py-Ir and HA-ss-Py-Ir nanoparticles containing 5 mg of Ir(III) were dispersed in PBS buffer (pH=7.4, or 5.0), and nanoparticle suspensions (1 mL) were transferred to dialysis tubes (MWCO 3500) and were then immersed in PBS buffer (pH=7.4, or 5.0, 20 mL) containing 0.1% (w/v) Tween 80 to achieve sink conditions. Reduction-responsive release media was produced by adding GSH to PBS buffer (pH=7.4) at final concentrations of 0, 10, and 20 mM. In addition, PBS (pH=5.0) containing 20 mM GSH was also tested as release medium. Release media were gently stirred in a water bath at 37°C, and 2 L aliquots were collected and replaced with equivalent volumes of fresh media at predetermined time intervals. Concentrations of Ir(III) released into the aqueous solution from HA-Py-Ir and HA-ss-Py-Ir in reductive and acidic environments were quantitatively analyzed using UV-Vis spectroscopy, and percentages of drug release were calculated by interpolation from a standard calibration curve. Release experiments were conducted in triplicate and the results are presented as means with standard deviations.

***In vitro* cytotoxicity studies**

Cell culture

A549 lung cancer cells were grown in DMEM containing 10% inactivated fetal bovine serum (FBS) and 1% penicillin-streptomycin. The same culture media were used in subsequent confocal microscopic observations and cell viability assays. All cells were maintained in a humidified incubator at 37°C with 5% CO_2.

The *in vitro* cytotoxicity of designed Ir-loaded micelles (HA-ss-Py-Ir, HA-Py-Ir) and HA-based micelles (HA-ss-Py, HA-Py) against A549 cells was evaluated using the 3-(4,5-dimethylthiazol-2-yl)-2,5-dipheny-ltetrazolium bromide (MTT) assay. Micelle samples were added at equivalent concentrations. A549 cells were seeded into 96-well plates at 5×10^3 per well in 100 μL of culture medium for 24 h and were then washed twice with PBS (pH=7.4) and treated with various concentrations of HA-ss-Py, HA-Py micelles, and free Ir(III), HA-ss-Py-Ir, and HA-Py-Ir nanoparticles for 48 h. Culture media were then removed and the cells were washed twice with PBS to remove the remaining treatments. Subsequently, MTT assay stock solution in PBS (25 μL, 5 mg/mL) was added to each well and the cells were incubated for 4 h. Unreacted MTT in the culture medium was carefully removed and purple formazan crystals in metabolically active cells were dissolved in DMSO (100 μL). Subsequently, absorbance of dissolved formazan dye was determined at 490 nm in each well using a microplate reader (EnSpire 2300, PerkinElmer, USA). Cell viabilities were determined according to the resulting optical density (OD_{sample}) values relative to those in control ($OD_{control}$), which were cells that were not treated, and were expressed as percentages of the control. Experiments were conducted in triplicate and standard deviations of independent experiments are presented as error bars.

In vitro cellular uptake and intracellular release of of nile red (NR) labeled HA-Py and HA-ss-Py micelles

The *in vitro* cellular uptake and intracellular release studies of micelles was investigated in A549 cells using confocal laser scanning microcopy (CLSM). The fluorescent probe nile red was encapsulated in micelles, and nile red loaded HA-Py and HA-ss-Py micelles were prepared with a similar protocol to that for Ir(III)-loaded nanoparticles. A549 cells were plated on microscope slides in 6-well plates at 1×10^5 cells/well with culture medium (2 mL) containing 10% FBS, penicillin (100 IU/mL), and streptomycin (100 μg/mL), and were incubated at 37°C in a humidified atmosphere containing 5% CO_2 for 24 h. Subsequently, nile red loaded HA-Py or HA-ss-Py nanoparticles (100 μL) were added to all the wells and were incubated for another 6 or 24 h. For competitive inhibition studies, A549 cells were pre-treated with free HA polymer (10 mg/mL) for 2 h and were then incubated with nile red loaded HA-ss-Py nanoparticles to confirm CD-44 mediated cell uptake.[60] Culture media were then removed and the cells were rinsed twice with PBS and fixed with 4% paraformaldehyde solution for 20 min. Finally, cell nuclei were stained with Hoechest 33342 for 10 min and the intracellular uptake of nanoparticles was determined using confocal laser scanning microscopy (Leica, UK) with excitation and emission wavelengths of 352 and 452 nm for Hoechest 33342, and 488 and 530 nm for nile red, respectively.

In vivo animal experiments and tumor models

Female Balb/c nude mice of 4-5 weeks of age were purchased from the Chinese Academy of Sciences (Shanghai). All animal experiments were performed in compliance with the guidelines approved by the Animal Ethics Committee of Shanghai Jiao Tong University. Tumor-bearing

mice were prepared by subcutaneously injecting 200 μL cell suspensions containing 1×10^6 A549 cells in PBS into the right armpit regions. Tumor volumes were allowed to reach approximately 200 mm^3 before experiments were carried out.

In vivo antitumor efficiency of HA-Py-Ir and HA-ss-Py-Ir nanoparticles

Antitumor efficiencies of nanoparticles were evaluated in A549 tumor-bearing mice. Mice were randomly divided into treatment groups, and received intravenous injections of HA-Py micelles, HA-ss-Py micelles, or HA-Py-Ir, HA-ss-Py-Ir, or free Ir(III) via tail veins at doses of 5 mg/kg Ir equivalents (200 μL), respectively, 10 times at 3 day intervals. Hydrophobic drugs are regularly dissolved in DMSO for biologic experments, both *in vitro* and *in vivo* in experimental models.[66, 67] Free Ir was dissolved in 10% DMSO-physiological saline considering the poor water solubility of Ir in water. In parallel, a control group received injections of a 10% DMSO-physiological saline. The protocol for antitumor efficiencies of nanoparticles was designed as described in a previous report.[67] Tumor sizes were measured using vernier calipers once every 3 days and the body weights of mice were recorded every 3 days throughout the experiment. Tumor volumes (V) were calculated using the following formula: V (mm^3) = 1/2 × longest diameter (mm) × shortest $diameter^2$ $(mm)^2$. At the end of the experiment, the mice were sacrificed and tumors were excised, weighed, and photographed.

In vivo and *ex vivo* imaging of Cy5.5-loaded HA-Py and HA-ss-Py nanoparticles

To monitor the *in vivo* distributions of nanoparticles, the NIR dye Cy5.5 was loaded into HA-Py and HA-ss-Py micelles and Cy5.5 loaded nanoparticles were prepared using a dialysis method according to the protocol for nile red loaded nanoparticles. A549 tumor-bearing mice were injected intravenously with 200 μL of Cy5.5-loaded HA-Py or HA-ss-Py self-assembled

nanoparticles via the tail veins at doses of 5 mg/kg. Fluorescent images of mice were obtained at appropriate wavelengths (λ_{ex}, 670 nm and λ_{em}, 700 nm) using an *in vivo* imaging system (Caliper IVIS Lumia II, Caliper life science, USA) at 1, 2, 4, 6, 8, and 12 h after injections. Calculations were performed using the region of interest (ROI) function of Analysis Workstation software (ART; Advanced Research Technologies Inc., Montreal, Canada).

Six hours after the injections, A549 tumor-bearing mice were sacrificed and tumor tissues and major organs, including the heart, liver, spleen, lung, and kidney, were excised. Subsequently, *ex vivo* fluorescent images of the tumor tissues and major organs were obtained and analyzed using the imaging system as described above. Tissue distributions of nanoparticles were quantified by measuring the fluorescence intensities at regions of interest (ROI).

Statistical analysis

Data are expressed as means ± standard deviations. Differences between experimental and control groups were identified using 2-tailed Student's t-tests and were considered significant when $p < 0.05$.

RESULTS AND DISCUSSION

Synthesis and characterization of [(η^5-Cp^{xbiph})Ir(phpy)(py)]PF$_6$

Initially, complexes 1 Cp^{xbiph}H, 2 [(η^5-Cp^{xbiph})IrCl$_2$]$_2$, 3 [(η^5-Cp^{xbiph})Ir(phpy)Cl], and 4 [(η^5-Cp^{xbiph})Ir(phpy)(py)]PF$_6$ were synthesized with moderate yields as described previously (Figure 1A). Reaction details are described in the "Materials and Methods" section. The compound [(η^5-Cp^{xbiph})Ir(phpy)(py)]PF$_6$ is one of the most potent anticancer complexes, and structures of

intermediates 1-3 and Ir(III) anticancer drug 4 were confirmed using ^{1}H-NMR spectroscopy (Figures 1B).

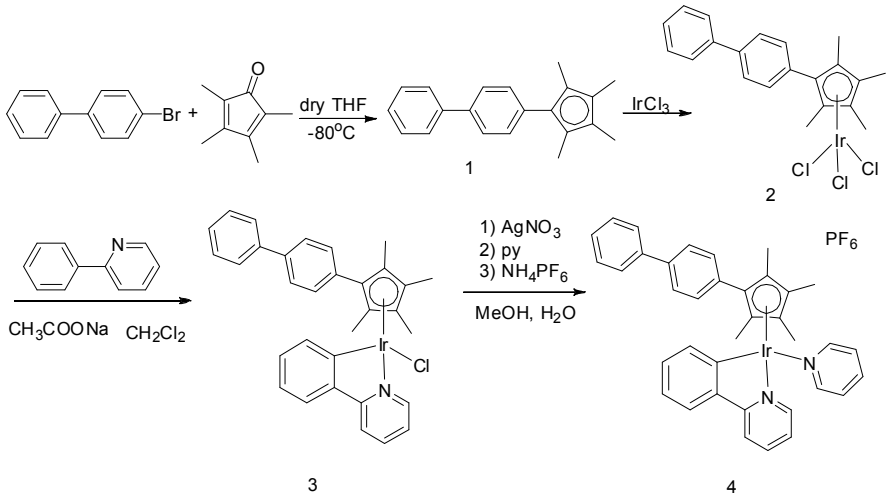

(A)

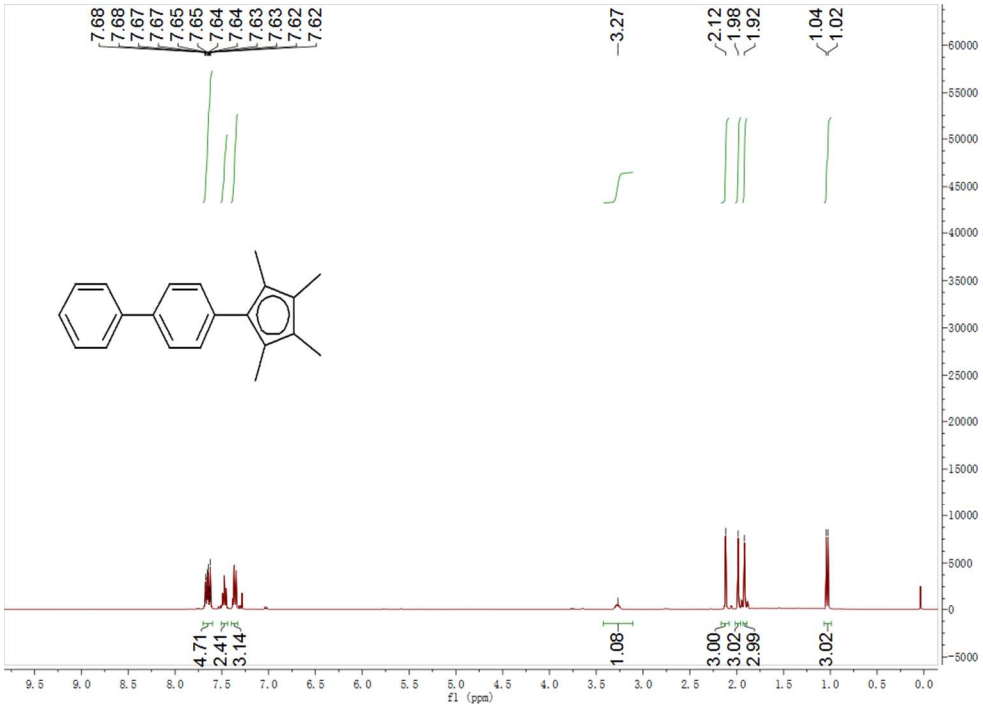

(a) ^{1}H-NMR spectra of $Cp^{xbiph}H$

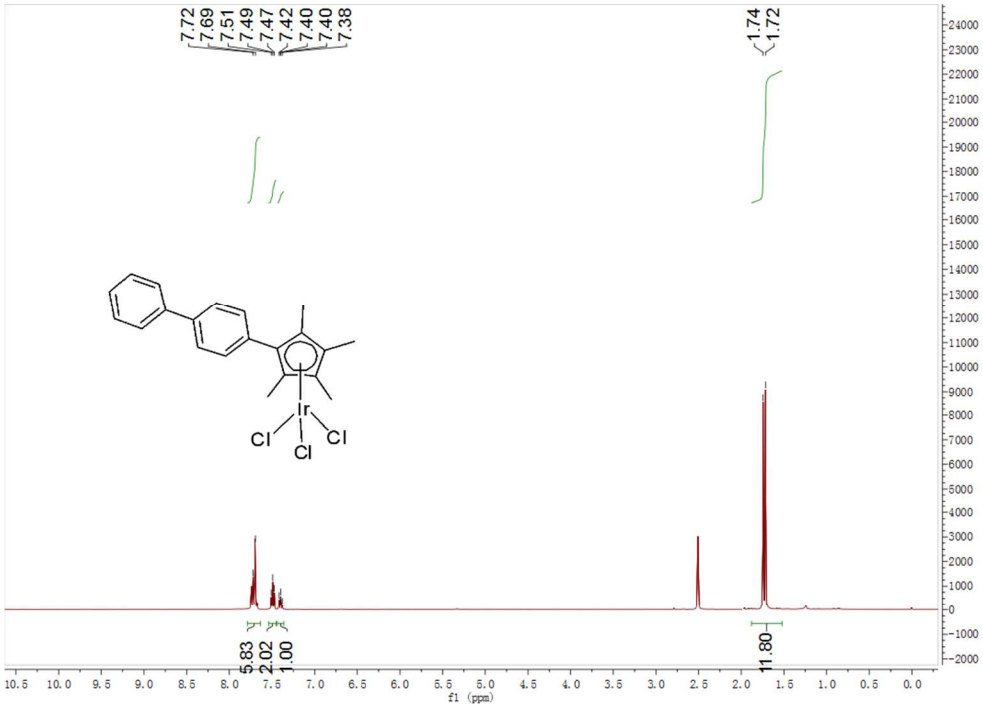

(b) ^{1}H-NMR spectra of $[(\eta^{5}\text{-Cp}^{\text{xbiph}})\text{IrCl}_2]_2$

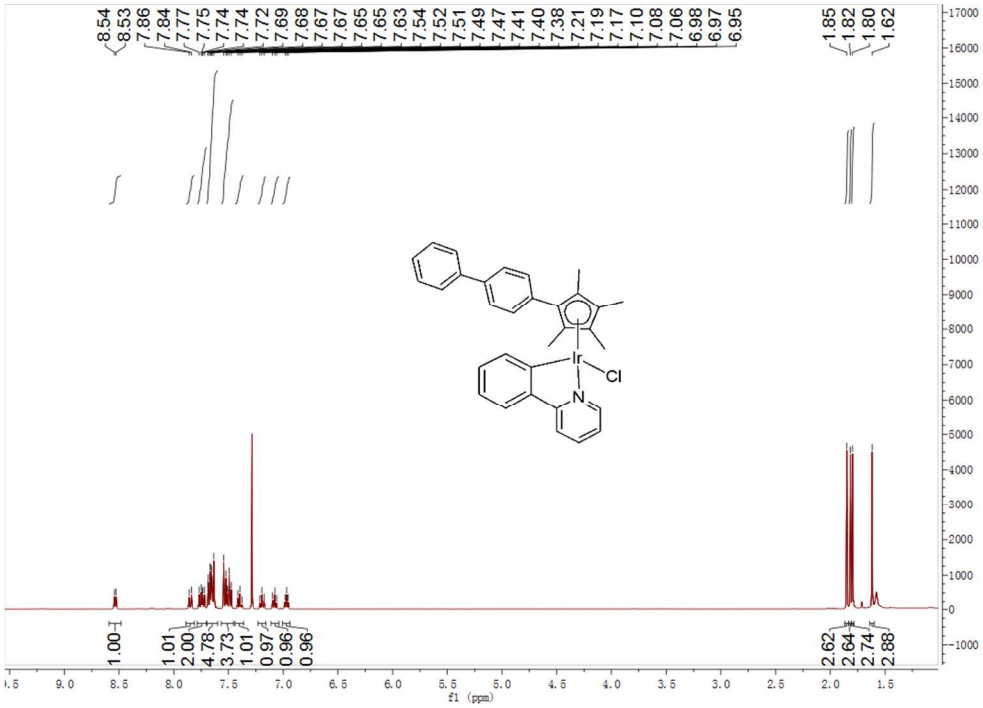

(c) ^{1}H-NMR spectra of $[(\eta^{5}\text{-Cp}^{\text{xbiph}})\text{Ir(phpy)Cl}]$

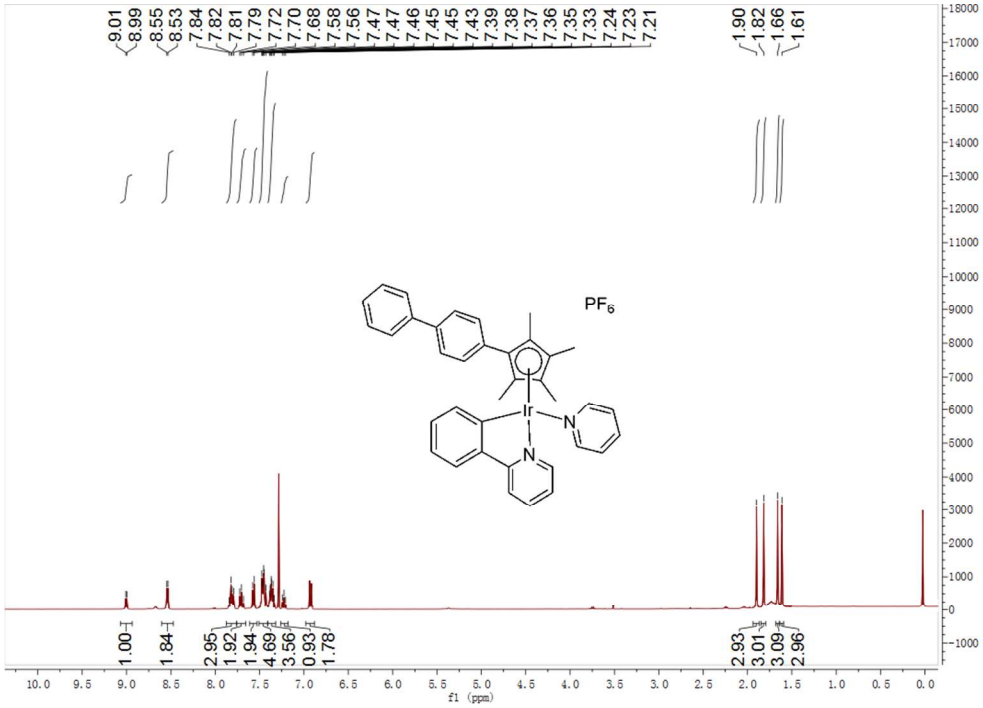

(d) ^{1}H-NMR spectra of [(η^5-Cp^{xbiph})Ir(phpy)(py)]PF$_6$

(B)

Figure 1. (A) Synthesis route for complexes 4 [(η^5-Cp^{xbiph})Ir(phpy)(py)]PF$_6$. (B) the ^{1}H-NMR spectra of complexes 1, 2, 3 and 4

Synthesis and characterization of HA-Py and HA-ss-Py conjugates

Figure 2A shows the protocol for the synthesis of HA-Py and HA-ss-Py conjugates. In this investigation, we developed a novel and tumor-targeting delivery vehicle that can be loaded with Ir(III) anticancer complexes and that can rapidly release them inside target cells. The ensuing reduction-sensitive amphiphilic HA-ss-Py conjugates were designed and prepared as follows: Firstly, HA-ss was synthesized by chemical conjugation of cystamine as a donor of disulfide bonds to hydrophilic HA polymers using EDC chemistry. Subsequently, pyrene groups, which are π-rich moieties for the loading and active release of Ir, were introduced to HA-ss conjugates

with free amines of cystamine through amide formation in the presence of EDC and NHS, resulting in the formation of HA-ss-Py conjugates. As a control, reduction-insensitive HA-Py was synthesized by the conjugation of 1-pyrenebutyric acid to the HA polymer using the symmetrical linker 1,4-diaminobutane in a carbodiimide-mediate coupling reaction.

The chemical structures of HA-diaminobutane, HA-ss, HA-Py, and HA-ss-Py conjugates were characterized using ^{1}H-NMR (Figure 2B). Compared with ^{1}H-NMR spectra of HA, distinct peaks were detected at δ = 1.65, 2.80, and 2.95 ppm and at δ = 2.78 and 2.93 ppm from ^{1}H-NMR spectra of HA-diaminobutane and HA-ss and were attributed to methylene protons from 1,4-diaminobutane and cystamine, respectively. These data confirmed the successful synthesis of HA-diaminobutane and HA-ss conjugates. In quantitative analyses, grafting efficiencies of 1,4-diaminobutane and cystamine were about 0.22 and 0.20 from the integration ratio of the peak of the methylene proton to that of the N-acetyl glucosamine proton peak of HA, which appeared at 2.0 ppm. Successful synthesis of HA-Py and HA-ss-Py conjugates were confirmed according to specific peaks from aromatic rings of pyrene (δ = 8.07-8.47; Figure 2B). According to integral ratios, degrees of substitution of pyrene groups in HA-Py and HA-ss-Py conjugates were 0.16 and 0.15, respectively.

The synthesis of HA derivatives was also characterized using FT-IR spectra (Figure 2C). In comparison with the spectra of HA, FT-IR spectra of HA-diaminobutane and HA-ss showed an additional peak at 1730 cm^{-1}, which was assigned to amide stretching vibration bands. Compared with the absorption spectra for HA-diaminobutane and HA-ss, spectra for HA-Py and HA-ss-Py included additional peaks at 847 cm^{-1}, and these corresponded with double bonds from pyrene groups. These data confirmed that pyrene was successfully conjugated to the

backbone of HA-diaminobutane and HA-ss and that HA derivatives were successfully synthesized.

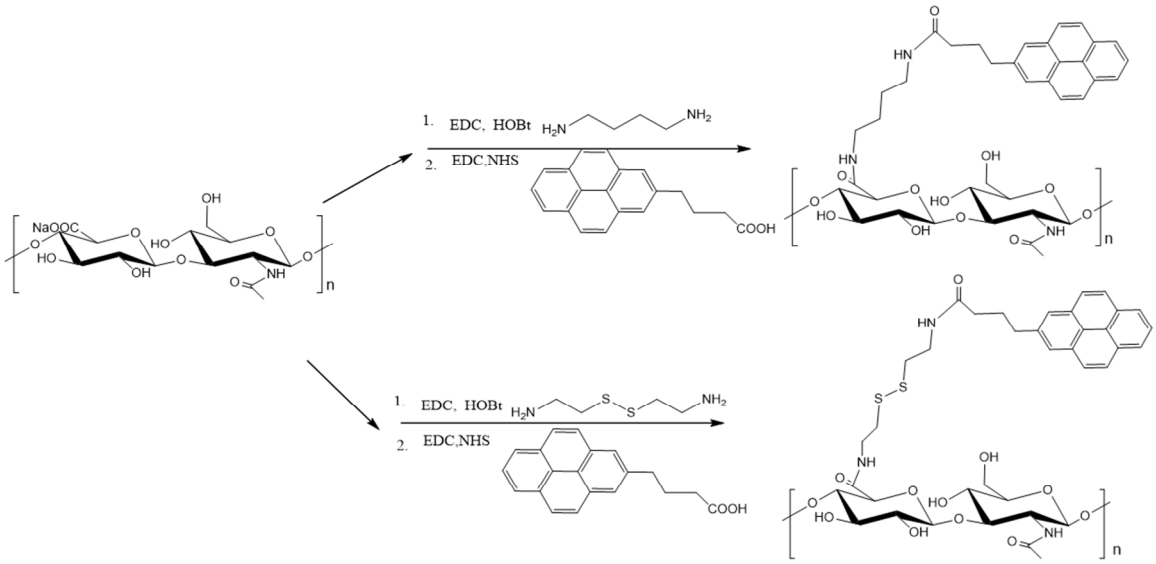

(A)

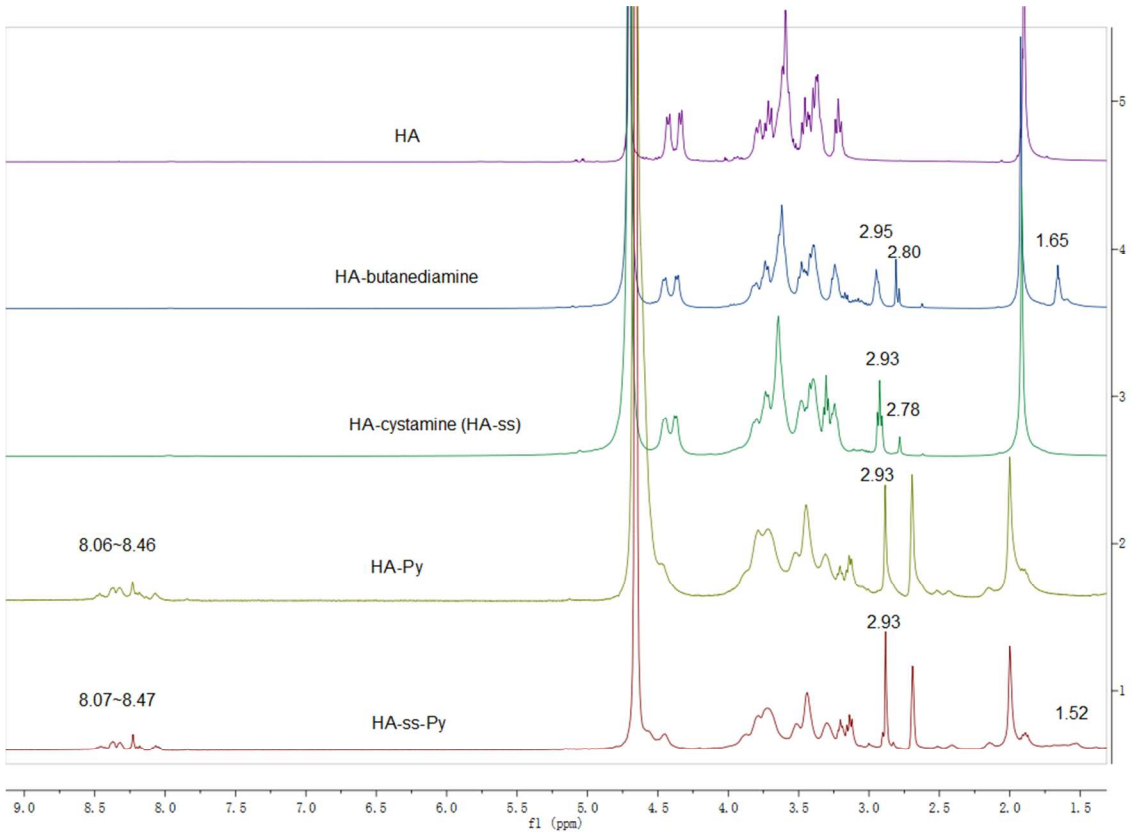
HA
HA-butanediamine
2.95
2.80
1.65
HA-cystamine (HA-ss)
2.93
2.78
HA-Py
8.06~8.46
2.93
HA-ss-Py
8.07~8.47
2.93
1.52
f1 (ppm)

(B)

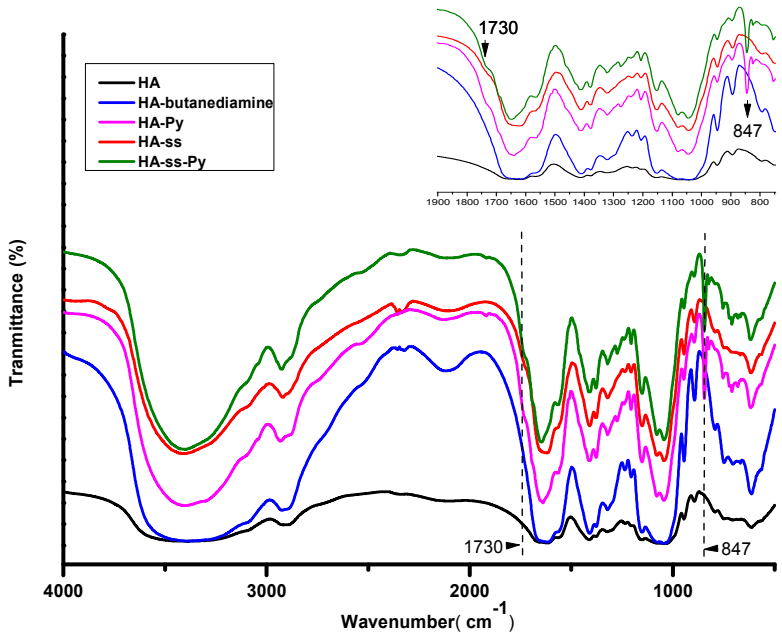

(C)

Figure 2. (A) The synthetic route for HA-Py and HA-ss-Py conjugates. (B) ^{1}H-NMR spectra of HA, HA-ss, HA-diaminobutane, HA-Py and HA-ss-Py conjugates. (C) FT-IR spectra of HA, HA-ss, HA-diaminobutane, HA-Py, and HA-ss-Py conjugates.

Preparation and characterization of HA-ss-Py and HA-Py micelles and Ir-loaded nanoparticles

Reduction-sensitive HA-ss-Py and reduction-insensitive HA-Py conjugates formed micelles via self-assembly in aqueous solution due to hydrophobic interactions between the pendant hydrophobic groups. HA-ss-Py and HA-Py micelles were prepared using a simple ultrasonic method. In general, the amphiphilic properties and self-assembly behaviors of micelles are characterized by measuring CMC using pyrene as a hydrophobic fluorescent probe. In Figure

3A, fluorescence intensity ratios ($\lambda_{374}/\ \lambda_{385}$) at λ_{ex} = 330nm are plotted against conjugate concentrations, and CMC were estimated from threshold concentrations of micelles. These experiments showed that the HA-ss-Py and HA-Py conjugates had low CMC of about 2.4 and 1.8 mg/L, respectively. These low CMC indicate that the present conjugates form particularly stable micelles under highly diluted conditions.

Particle size distributions and zeta potentials of nanoparticles play important roles in intravenous activities. Figure 3B and 3C show the DLS results with TEM and AFM images for HA-ss-Py and HA-Py micelles. DLS results showed that reduction-sensitive HA-ss-Py micelles had an average particle size of 260 ± 20 nm and a low polydispersity index (PDI) of 0.241 in PBS (pH=7.4). Under the same conditions, HA-Py micelles had a mean particle size of 250 ± 15 nm and a PDI of 0.238 (Table 1). The ζ potentials of HA-ss-Py and HA-Py micelles indicated negative charges of −24.6 ± 0.4 and −25.9 ± 0.5 mV, respectively, reflecting charged carboxylic groups of HA polymers on micelle surfaces. These negatively charged surfaces inhibit the aggregation of micelles by electrostatic repulsion and provide long-term stability in aqueous solution. Compared to the sizes of HA-ss-Py and HA-Py micelles at pH=7.4, no size changes were also evident for HA-ss-Py (average particle size = 267 ± 22 nm) and HA-Py micelles (average particle size = 248 ± 13 nm) at pH=5.0 (Figure 3(B)). TEM and AFM micrographs revealed that these micelles were generally spherical, with sizes that were in accordance with DLS results. The average size of HA-ss-Py and HA-Py micelles was approximately 120 nm (Figure 3C). TEM and AFM images indicated micelle sizes that were smaller than those determined by DLS, likely reflecting swelling of hydrophilic backbone in aqueous solution.[68]

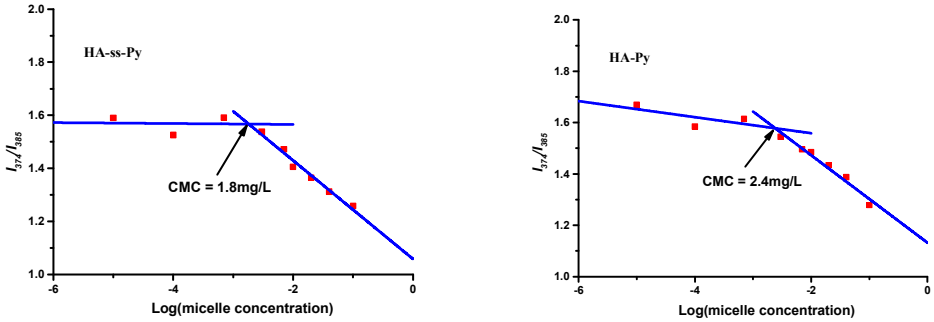
HA-ss-Py
CMC = 1.8mg/L
Log(micelle concentration)
HA-Py
CMC = 2.4mg/L
Log(micelle concentration)

(A)

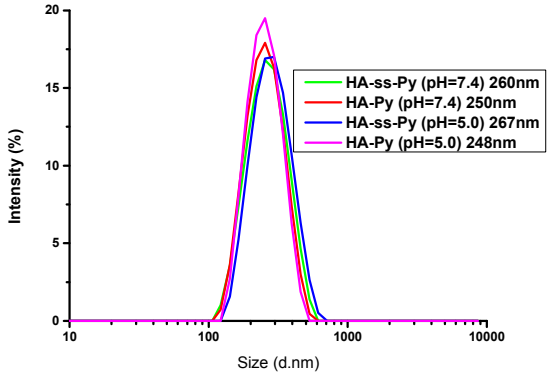
HA-ss-Py (pH=7.4) 260nm
HA-Py (pH=7.4) 250nm
HA-ss-Py (pH=5.0) 267nm
HA-Py (pH=5.0) 248nm
Intensity (%)
Size (d.nm)

(B)

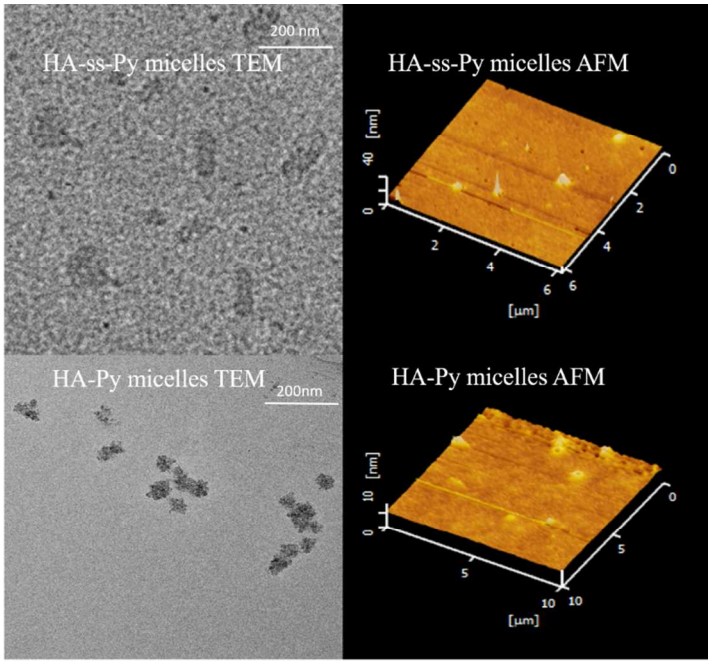

(C)

Figure 3. (A) CMC determination of HA-Py and HA-ss-Py micelles. (B) DLS results of HA-ss-Py and HA-Py micelles. (C) AFM and TEM images of HA-ss-Py and HA-Py micelles

Stability of HA-based micelles

In order to investigate the stability of HA-based micelles, we determined changes in the sizes of HA-Py and HA-ss-Py micelles using DLS in the presence or absence of GSH at 2 µm, 10 mM, and 20 mM. As shown in Figure 4A, HA-ss-Py micelle particle sizes increased significantly from 260 nm to 350 nm and 580 nm after 24 h in the presence of 10 and 20 mM GSH, respectively. These observations suggest that cleavage of disulfide linkages led to the aggregation of micelles. However, no size changes were evident for HA-ss-Py micelles after 24 h in the presence of 2 µM GSH, which is the GSH concentration in extracellular fluids.[69] In contrast, sizes of HA-Py micelles did not vary with GSH concentrations after 24 h, suggesting

that HA-Py micelles have a good aqueous stability during circulation. As shown in Figure 4B, HA-ss-Py micelle particle sizes increased significantly with time in the presence of 20 mM GSH, and these observations were accompanied by decreased scattering intensities.

Preparation and characterization of Ir(III)-loaded HA-ss-Py and HA-Py nanoparticles

Because the Ir(III) anticancer drug has diphenyl structures, and HA-based micelles contain pyrene structures, the Ir anticancer drug can be loaded into HA-ss-Py and HA-Py micelles via π–π stacking interactions. Thus, encapsulation of Ir(III) anticancer drug was achieved using simple dialysis. Because nanoparticle sizes and ζ potentials of drug-loaded nanoparticles are key factors in intravenous administration, we performed further DLS studies (Figure 4C) and showed average hydrodynamic diameters of HA-ss-Py-Ir and HA-Py-Ir nanoparticles of 210 ± 3 and 230 ± 5 nm (pH=7.4) with low polydispersity indexes of 0.084 and 0.100, respectively. After loading the Ir(III) anticancer drug, nanoparticles sizes were diminished to 30-40 nm, reflecting the compact structure of π–π stacking interactions between Ir(III) anticancer and pyrene substituents. In addition, ζ potentials of HA-ss-Py-Ir and HA-Py-Ir nanoparticles were negative at pH=7.4 (−25.1 ± 0.2 and −21.0 ± 0.3 mV, respectively), offering significant repulsion between nanoparticles and increased stability (Table 1). To investigate the stability of HA-ss-Py-Ir and HA-Py-Ir nanoparticles, we determined the changes in the sizes of HA-Py-Ir and HA-ss-Py-Ir nanoparticles using DLS in the presence of GSH of 0, 2 μM, 10 mM, and 20 mM at pH=7.4. As shown in Figure 4C, upon addition of 10 mM and 20 mM GSH, HA-ss-Py-Ir nanoparticles exhibited significant increase in particle size. In contrast, little size changes were observed for HA-Py-Ir nanoparticles, and for HA-ss-Py-Ir nanoparticle in the presence of 0 and 2 μm GSH. Moreover, the DLS results also showed that the HA-ss-Py-Ir and HA-Py-Ir nanoparticles were destabilized at pH=5.0 forming relatively large micelles of ca 300 nm. These results implied that

the HA-ss-Py-Ir and HA-Py-Ir nanoparticles might be triggered to release Ir(III) anticancer drug in acidic environment, which was further confirmed in the following *in vitro* pH-sensitive release experiments.

In further experiments, we examined nanoparticle morphologies of HA-ss-Py-Ir and HA-Py-Ir using TEM and AFM (Figure 4D). TEM and AFM micrographs showed spherical morphologies with particle sizes of about 100 nm, and the differences in comparison with DLS data likely reflect swelling of nanoparticles in aqueous solution.

The functionalization process of Ir(III) anticancer drug loaded HA-ss-Py and HA-Py were monitored by UV-Vis absorption spectroscopy. As shown in Figure 4E, Ir anticancer drug in ethanol/water (1:1 v/v) showed one absorption at 263 nm. When Ir loaded on either HA-ss-Py or HA-Py formed HA-ss-Py-Ir or HA-Py-Ir nanoparticles, the absorance peaks at 263nm slightly shifted to 266 nm, indicative of interactions between Ir and Py groups in HA conjugates. The optical results indicated that Ir(III) had been loaded on the HA-based micelles as expected.

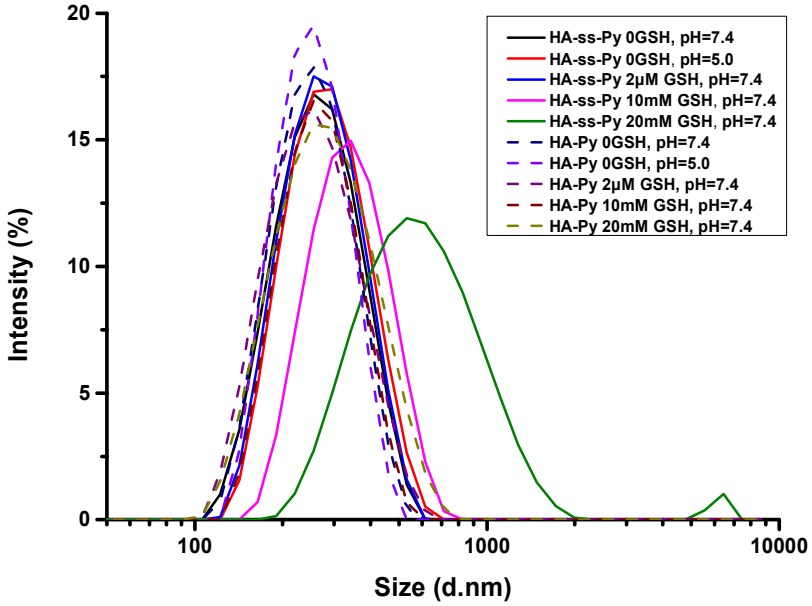

(A)

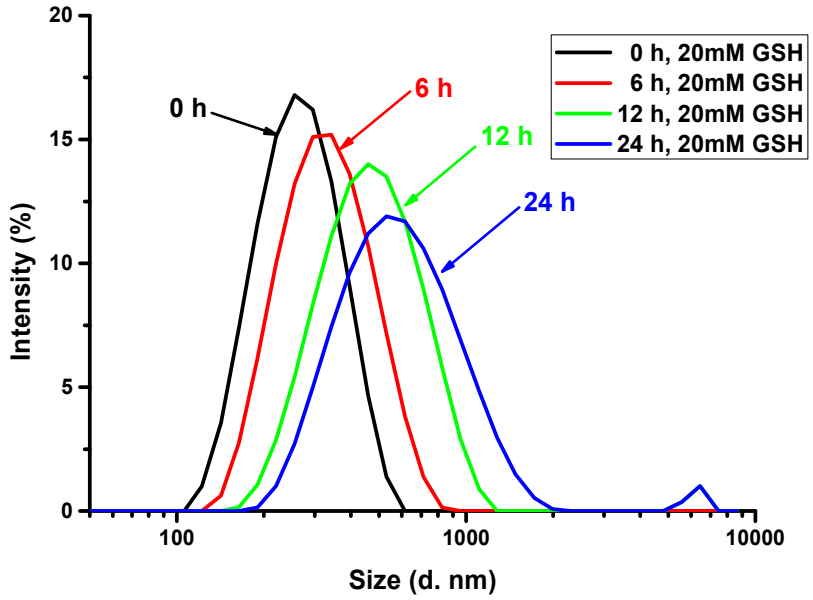
0 h, 20mM GSH
6 h, 20mM GSH
12 h, 20mM GSH
24 h, 20mM GSH
0 h
6 h
12 h
24 h
Intensity (%)
Size (d. nm)
20
15
10
5
0
100
1000
10000

(B)

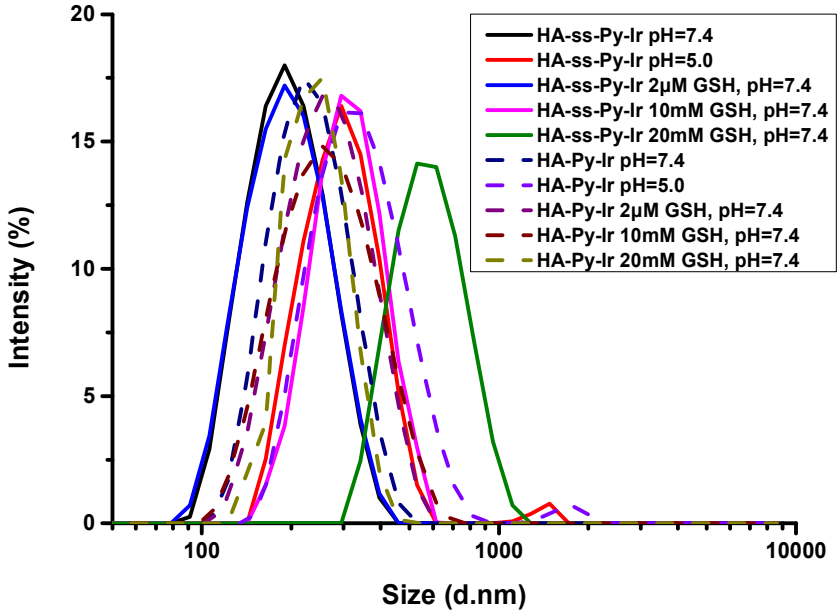
HA-ss-Py-Ir pH=7.4
HA-ss-Py-Ir pH=5.0
HA-ss-Py-Ir 2μM GSH, pH=7.4
HA-ss-Py-Ir 10mM GSH, pH=7.4
HA-ss-Py-Ir 20mM GSH, pH=7.4
HA-Py-Ir pH=7.4
HA-Py-Ir pH=5.0
HA-Py-Ir 2μM GSH, pH=7.4
HA-Py-Ir 10mM GSH, pH=7.4
HA-Py-Ir 20mM GSH, pH=7.4
Intensity (%)
Size (d.nm)
20
15
10
5
0
100
1000
10000

(C)

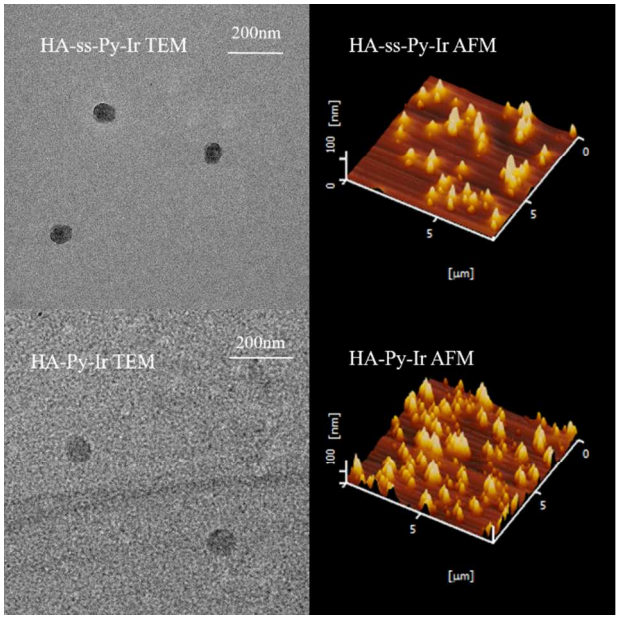
HA-ss-Py-Ir TEM
200nm
HA-ss-Py-Ir AFM
[nm]
100
0
5
5
0
[μm]
HA-Py-Ir TEM
200nm
HA-Py-Ir AFM
[nm]
100
0
5
5
0
[μm]

(D)

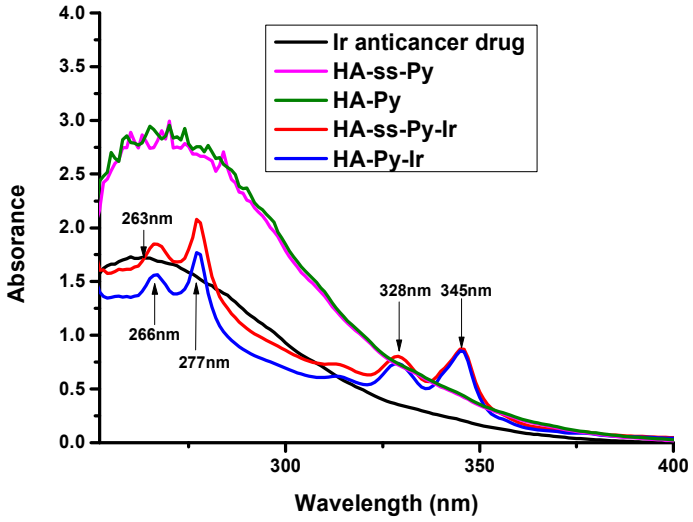
Ir anticancer drug
HA-ss-Py
HA-Py
HA-ss-Py-Ir
HA-Py-Ir
Absorance
Wavelength (nm)
263nm
266nm
277nm
328nm
345nm
4.0
3.5
3.0
2.5
2.0
1.5
1.0
0.5
0.0
300
350
400

(E)

Figure 4. (A) Size distribution of HA-ss-Py and HA-Py nanoparticles without GSH at pH=5.0, and in the presence of 0, 2 μM, 10mM and 20 mM GSH at pH=7.4. (B) Changes of particle sizes of HA-ss-Py micelles with time in response to 20mM GSH. (C) Size distribution of Ir-loaded HA-ss-Py and HA-Py nanoparticles without GSH at pH=5.0, and in the presence of 0, 2 μM, 10 mM and 20 mM GSH at pH=7.4. (D) TEM and AFM images of Ir(III)-loaded HA-ss-Py (A and B) and HA-Py nanoparticles (C and D). (E) UV-Vis absorption spectra of Ir(III) anticancer drug, HA-ss-Py, HA-Py, HA-ss-Py-Ir and HA-Py-Ir in ethanol/water (1:1 v/v).

After loading Ir(III) anticancer drug into micelles, the loading contents and efficiencies were determined using UV-Vis spectrophotometry (Table 1). In these experiments, both HA-ss-Py and HA-Py micelles had similar drug loading levels, with drug loading contents of 34.2% ± 0.7% and 35.9% ± 0.5%, and drug loading efficiencies of 78% ± 1.5% and 84% ± 2.0%, respectively.

Table 1 Characteristics of HA-ss-Py, HA-Py micelles, HA-ss-Py-Ir and HA-Py-Ir nanoparticles in PBS at pH 7.4

Entry	Mean diameter (nm)	Polydispersity index (PDI)	Zeta potential (mV)	Drug loading content (%)	Drug loading efficiency (%)
HA-ss-Py	260 ± 20	0.241	-24.6 ± 0.4	-----	-----
HA-Py	250 ± 15	0.238	-25.9 ± 0.5	-----	-----
HA-ss-Py-Ir	230 ± 5	0.084	-25.1 ± 0.2	34.2 ± 0.7	78 ± 1.5

HA-Py-Ir	210 ± 3	0.100	-21.0 ± 0.3	35.9 ± 0.5	84 ± 2.0

Values are mean ± standard deviation (SD) (n = 3)

***In vitro* reduction and pH-sensitive release of Ir anticancer drug from HA-ss-Py and HA-Py micelles**

The *in vitro* reduction-triggered release of Ir(III)-loaded HA-Py and HA-ss-Py micelles was investigated using dialysis analyses (MWCO = 3500 Da) in PBS buffer (pH=7.4, 0.1 M) at 37°C. Dialysis tubes contained 0.1% (w/v) Tween 80, and GSH was added to simulate the reductive microenvironments of the cytosol and the cell nucleus. Because disulfide linkages are readily broken in the presence of reducing agents, we assumed that disulfide-containing micelles would be responsive to the reducing agent GSH.

Cumulative release profiles of the Ir(III) anticancer drug from HA-based nanoparticles were monitored over time (Figure 5) and showed differing release profiles of HA-ss-Py and HA-Py micelles under reducing (presence of GSH) and nonreducing environments (absence of GSH). Final release of Ir(III) anticancer drug from HA-ss-Py micelles was approximately 10% after incubation for 48 h in the absence of GSH, but was about 40% in the presence of 10 mM GSH (intracellular GSH level) at the same time point. Moreover, Ir anticancer drug was rapidly released in the presence of 20 mM GSH, indicating reductive release of Ir(III). Under these conditions, approximately 70% of Ir(III) anticancer drug was released after 4 h and more than 95% of Ir(III) was released after 48 h. In contrast, drug release (ca. 10%) from HA-Py micelles was minimal after 48 h in the presence of 20 mM GSH, and this value was similar to that of HA-ss-Py micelles under nonreducing conditions. Similar results have also been observed for other HA crosslinked nanoparticles.[40, 70]

These release experiments indicate that HA-ss-Py micelles have superior colloidal stability under physiological conditions and can avoid premature drug release in circulation. In agreement, previous studies show prolonged circulation of nanoparticles that are stable under physiological conditions.[71] The facilitated drug release from HA-ss-Py micelles in the presence of 20 mM GSH likely reflects the reductive cleavage of disulfide cross-links, allowing increased diffusion from nanoparticles and facilitated drug release. In addition, these experiments suggest that the release of Ir(III) anticancer drug from HA-ss-Py micelles is triggered after internalization by cancer cells (reductive environment). Thus, HA-ss-Py micelles have potential as targeted delivery vehicles that may achieve the rapid intracellular release of Ir(III) anticancer drug and enhanced therapeutic efficacy.

The acidic conditions of tumor cells may also be exploited to facilitate specific drug delivery. Thus, we investigated the *in vitro* pH-sensitive release of Ir(III) anticancer drug from HA-ss-Py and HA-Py micelles (Figure 5). In these experiments, Ir(III) release was stimulated by acidic conditions, particularly in the initial phase, and these observations could be attributed to π–π stacking interactions between Ir and pyrenyl groups on the HA backbone. These data may also reflect degradation of the HA backbone under acidic conditions, further contributing to drug release.[72]

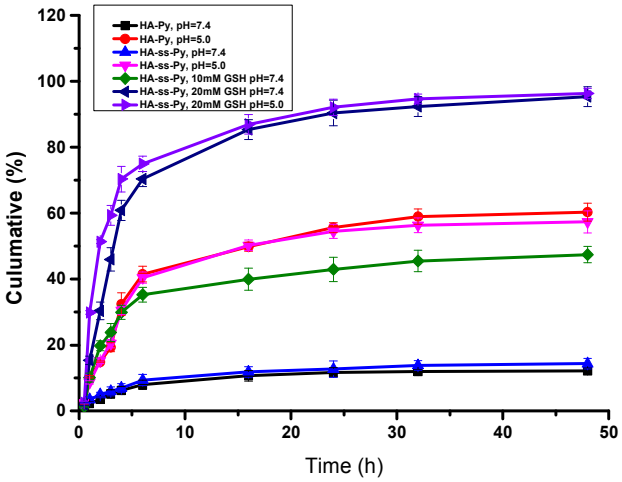

Figure 5. *In vitro* GSH and pH-triggered release test of Ir(III) anticancer drug from HA-Py and HA-ss-Py nanoparticles. Each point represents as mean ± SD (n = 3).

In vitro cytotoxicity studies

Cytotoxic activities of HA-Py and HA-ss-Py micelles were evaluated using MTT assays in A549 cells. As shown in Figure 6A, HA-ss-Py and HA-Py micelles showed no obvious cytotoxicity in A549 cells after 48 h, even at the tested nanoparticle concentration of 0.06 mg/mL. This biocompatibility further supports the potential of these nanoparticles as effective targeting vehicles for Ir(III) drug delivery to tumor sites.

In subsequent experiments, cytotoxic activities of free Ir(III), HA-ss-Py-Ir, and HA-Py-Ir nanoparticles were evaluated (Figure 6B) after 48h treatments of A549 cells. In particular, Ir(III)-loaded HA-based nanoparticles were significantly more toxic to A549 cells than free Ir(III) under identical conditions, and likely indicated a greater uptake of Ir(III) via CD44 receptor-mediated endocytosis. Moreover, the cytotoxic activities of nanoparticles increased with Ir(III) concentrations, with half maximal inhibitory concentration (IC_{50}) values for reduction-

sensitive HA-ss-Py-Ir, reduction-insensitive HA-Py-Ir, and free Ir(III) of 0.1, 0.15, and 0.56 $\mu g/mL^{-1}$, respectively. Taken together, the present data show that HA-ss-Py micelles have good biocompatibility, and release drugs in response to the intracellular reduction and pH environments. These properties are highly promising for targeted drug delivery.

Cellular uptake and intracellular release

To evaluate the intracellular uptake characteristics and release behaviors, A549 cells were treated with nile red labeled HA-based nanoparticles and were analyzed using CLSM. Human nonsmall cell lung adenocarcinoma (A549) cell lines are known to overexpress the CD44 receptors specific for HA.[73, 74] We performed CLSM after incubating cells with nile red-labeled HA-based nanoparticles for 6 h and 24 h. Nuclei were stained using Hoechest 33342. Nile red is an excellent fluorescent hydrophobic probe for the detection of intracellular lipid droplets by fluorescence microscopy. It was noteworthy that only free nile red molecules could detect lipid droplets.[75] Therefore, nile red released from HA-bassed micelles into the cytosol can exert its staining. This experiment was carried out to further evaluate the drug release behavior of these HA-based micelles. As shown in Figure 6C, strong fluorescence was detected in A549 cells after 6 h-treatments with HA-ss-Py and HA-Py micelles, indicating successful and efficient cellular internalization and and intracellular release of HA-based micelles. However, the fluorescence intensities of A549 cells after 24h treatments with HA-based nanoparticles were decreased, implying that the fluorescence was partially quenched in cytosol. Furthermore, nile red labeled HA-ss-Py nanoparticles had a greater fluorescence than HA-Py nanoparticles after 6 and 24 h treatments of A549 cells, further indicating that HA-ss-Py micelles mediate highly efficient intracellular drug release. In addition, pretreatment of A549 cells with excess HA strongly inhibited the subsequent cellular uptake of HA-based micelles, indicating saturation of CD44 by

HA. Finally, chemical modification of HA did not affect receptor-mediated uptake of HA through CD44, indicating that HA-ss-Py micelles can be used for targeted delivery and rapid drug release in cancer cells.

Cellular uptake of nanoparticles through endocytosis is crucial for drug delivery and nanomedicine, which is often affected by the size and shape of nanoparitcles.[76] Many studies have suggested that the optimial sizes of nanoparticles for endocytosis are less than ~100nm.[76, 77] However, many researchers have focused on investigating the polymer nanoparticles for drug delivery, which are generally larger than 100nm.[78] In this study, the cellular uptake of HA-based nanoparticles with ~250nm size should be related to the modified HA molecules that can specifically target A549 cells via the CD44 receptor-mediated pathway.[79, 80]

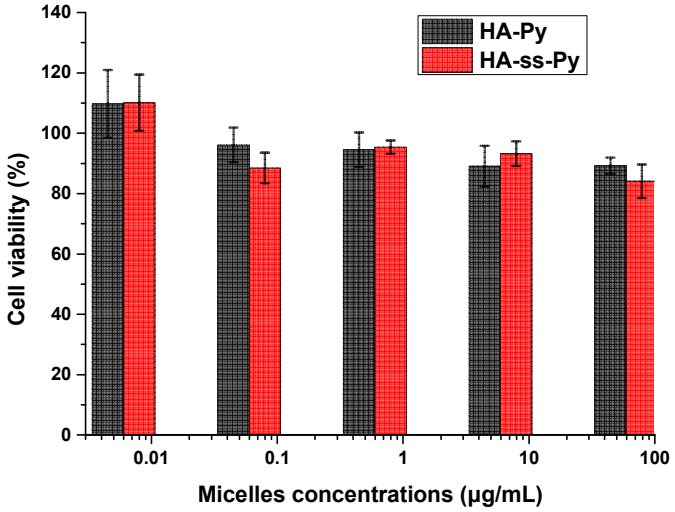

(A)

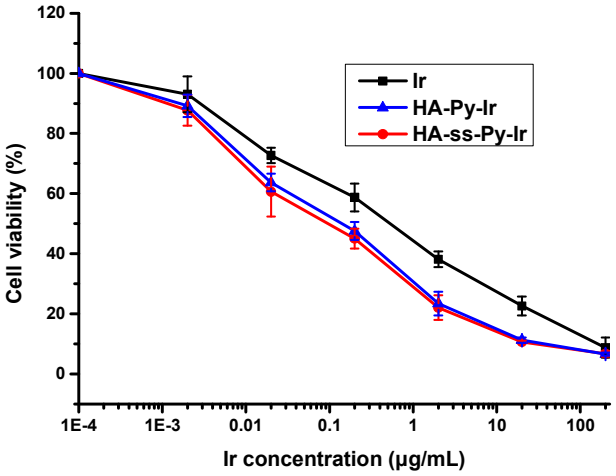

(B)

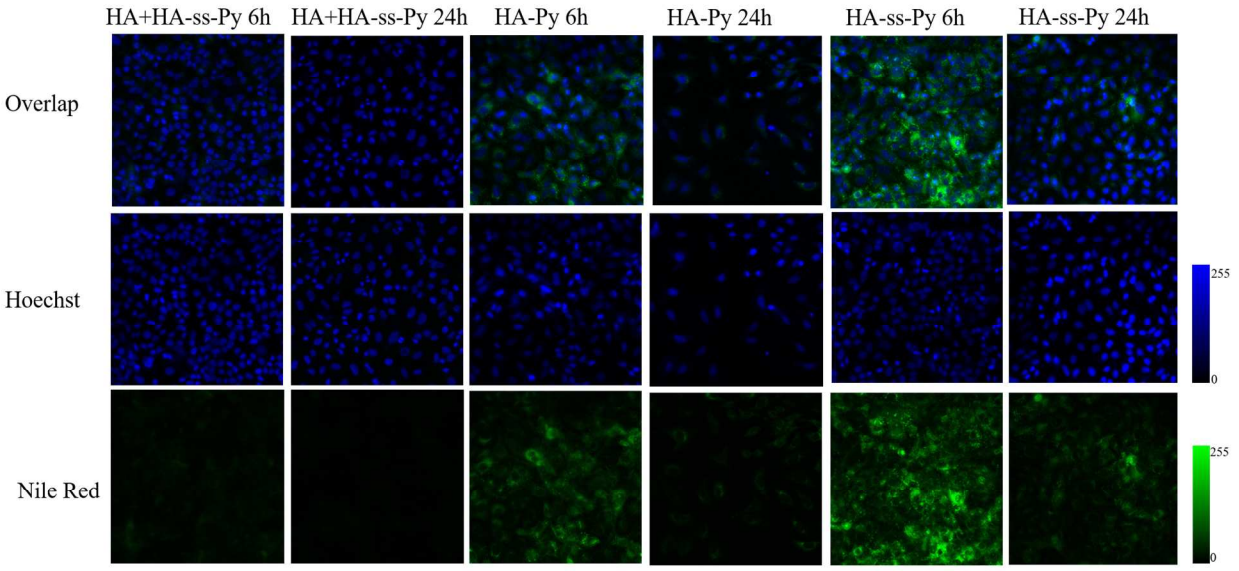

(C)

Figure 6. (A) Cytotoxicity of HA-ss-Py and HA-Py micelles to A549 cells. (B) Cytotoxic activities of Ir(III), Ir(III)-loaded HA-ss-Py and HA-Py nanoparticles to A549 cells. Data are presented as the average ± standard deviation (n=3). (C) *In vitro* cellular uptake studies of nile

red labeled HA-based nanoparticles in A549 cells. Nile red labeled HA-based nanoparticles were incubated for 6 h and 24h, respectively. Cellular uptake and distribution of Nile red labeled HA-based nanoparticles were examined by CLSM. Green and blue colors indicate nile red and Hoechest 33342, respectively.

***In vivo* antitumor therapeutic efficacy and safety**

The *in vivo* therapeutic efficacy of Ir(III)-loaded HA-based nanoparticles was determined in A549 tumor-bearing female Balb/c nude mice. After growth of tumors to about 200 mm^3, mice were treated with HA-based micelles, Ir(III)-loaded HA-based nanoparticles, or 10% DMSO-physiological saline (control), and the tumor volumes and body weights of tumor-bearing mice were measured every 3 days for 30 days. Tumor volumes increased dramatically in the untreated group throughout the experimental period, and no significant differences in tumor growth profiles were observed between the control, HA-ss-Py, and HA-Py micelle treatment groups (Figure 7A). Moreover, no body weight loss was observed in these treatment groups (Figure 7B), suggesting negligible systemic toxicity and satisfactory safety of HA-ss-Py and HA-Py micelles at the present concentrations, as indicated in the *in vitro* cytotoxicity assays.

To determine the antitumor efficacy, free Ir(III), HA-ss-Py-Ir, and HA-Py-Ir nanoparticles were administered to A549 tumor-bearing female Balb/c nude mice *via* intravenous tail vein injections. As compared with free Ir treated mice, those treated with HA-ss-Py-Ir or HA-Py-Ir nanoparticles showed significantly suppressed tumor growth (Figure 7A), reflecting comparatively poor solubility and bioavailability of free Ir(III) anticancer drug. In addition, the anti-tumor activity of HA-ss-Py-Ir nanoparticles was greater than that of HA-Py-Ir nanoparticles (Figure 7A), with tumor inhibition rates of 60%, 89%, and 92% in free Ir(III), HA-ss-Py-Ir, and

HA-Py-Ir treatment groups, respectively. Moreover, tumor-bearing mice did not lose weight during treatments with HA-ss-Py-Ir and HA-Py-Ir, suggesting minimal systemic toxicity of these nanoparticles (Figure 7B). Results from real time monitoring of tumor sizes over 30 days are shown in Figure 7C. Mice were sacrificed and the tumors were excised after 30 days, and compared, and those treated with HA-ss-Py-Ir had the smallest tumor sizes (Figure 7D). Cumulatively, the present data indicate that HA-ss-Py-Ir has the highest anti-tumor therapeutic efficacy, and confirm that HA targeting and reduction-triggered drug release are effective strategies for improved tumor inhibition.

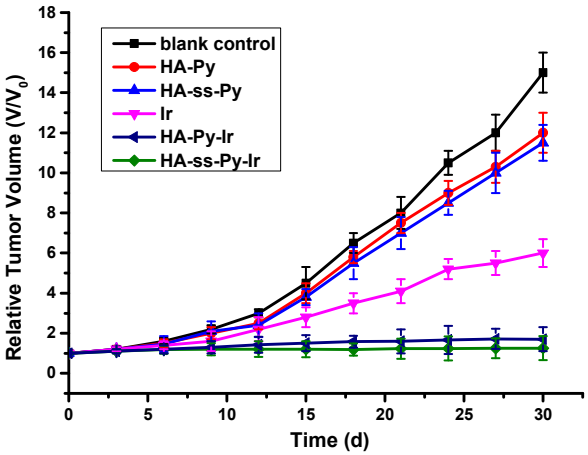

(A)

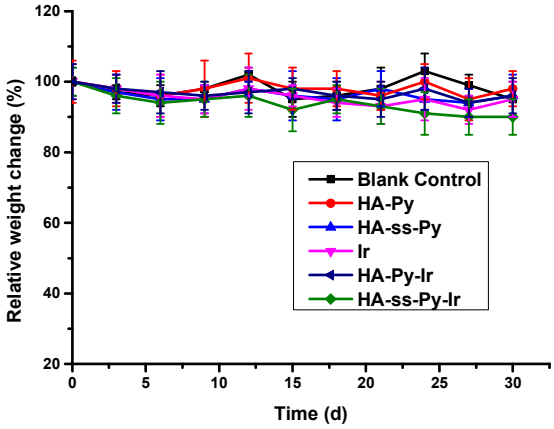
Relative weight change (%)
Time (d)
Blank Control
HA-Py
HA-ss-Py
Ir
HA-Py-Ir
HA-ss-Py-Ir

(B)

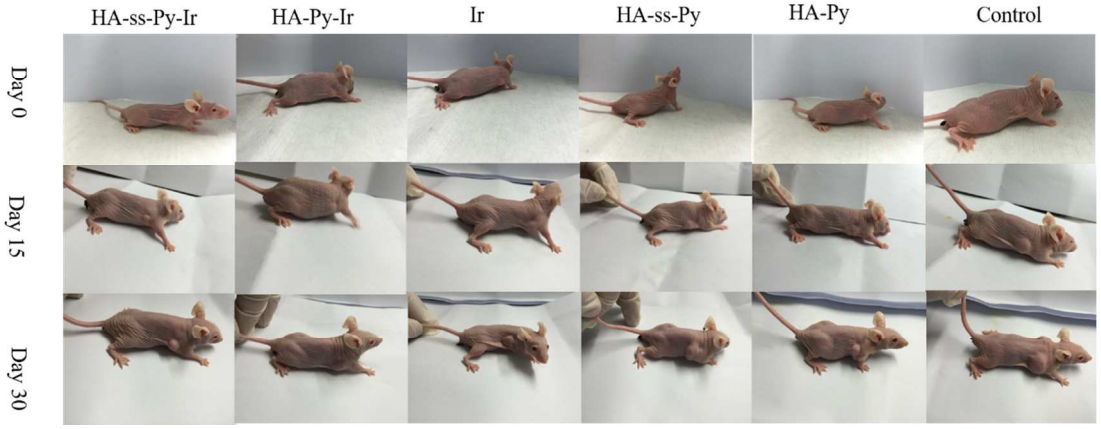
HA-ss-Py-Ir
HA-Py-Ir
Ir
HA-ss-Py
HA-Py
Control
Day 0
Day 15
Day 30

(C)

(D)

Figure 7. *In vivo* anti-tumor efficacy test in A549 tumor-xenografted mouse model. (A) Changes of tumor volumes (mm^3) after intravenous injection of 10% DMSO-physiological saline, HA-ss-Py, HA-Py, free Ir(III), HA-ss-Py-Ir and HA-Py-Ir nanoparticles. The injected dose was normalized to 5 mg/kg Ir. (B) Body weight (g) with tumor volume was monitored for 30 days. Data are presented as mean ± SD (n=3). (C) The mice were treated with different formulations and the tumor size was real-time monitored during the 30-day evaluation period. (D) Pictures of tumors in the blank control, HA-ss-Py, HA-Py, free Ir(III), HA-ss-Py-Ir and HA-Py-Ir nanoparticles groups.

In vivo and *ex vivo* imaging analyses

To evaluate the tumor-targetability and *in vivo* bio-distribution of HA-based nanoparticles, A549 tumor-bearing mice were injected with Cy5.5-labeled HA-ss-Py (a) and HA-Py (b) were investigated using a non-invasive near infrared optical imaging technique (NIRF). A549 tumor-bearing mice were monitored for 12 h after intravenous injections of Cy5.5-labeled HA-based

nanoparticles. As shown in Figure 8A, clear signals were observed in mice as early as 4 h after administering injections of either nanoparticles, and live imaging analyses showed that maximal fluorescent signals for both micellar formulations occurred at 6 h. In further experiments, bio-distributions of HA-based nanoparticles were examined in tumor xenograft mice using *ex vivo* fluorescence imaging of tumors and organs 6 h following injections of Cy5.5-labeled nanoparticles. As shown in Figure 8B, Cy5.5-labeled nanoparticles accumulated in tumors 6 h after the injections. Nanoparticle accumulation in the liver may indicate binding of HA to HARE receptors on liver sinusoidal endothelial cells.[81] In contrast, accumulation of micelles at tumor sites reflects the EPR effect and the receptor mediated uptake of micelles. These data further indicate that the present micelles mediate tumor-specific Ir drug delivery. Finally, fluorescence signals of HA-ss-Py micelles in tumors were relatively stronger than those of HA-Py micelles, indicating the promising effects and enhanced accumulation of HA-ss-Py micelles in tumors. These imaging data are consistent with the present *in vitro* cellular uptake studies and indicate that HA-ss-Py micelles are highly efficient Ir delivery vehicles that could be used to enhance tumor-targeting capabilities.

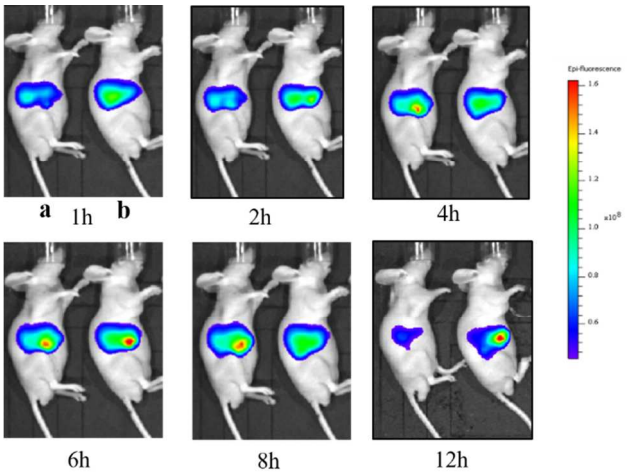

(A)

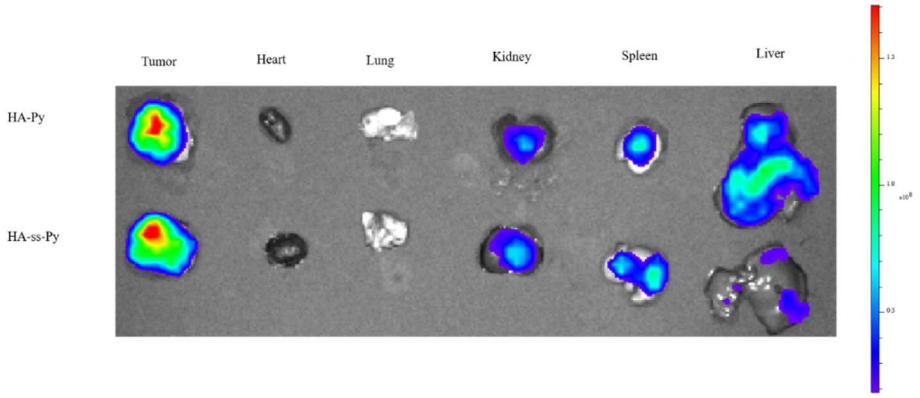

(B)

Figure 8. (A) *In vivo* near infrared fluorescent imaging of the A549 bearing mice after administration with Cy5.5-labeled HA-ss-Py (a), HA-Py (b). (B) *Ex vivo* fluorescence images of excised tissues including heart, liver, lung kidney spleen, and tumor at 6 h post-injection.

CONCLUSION

Two amphiphilic polymers of HA-ss-Py and HA-Py were successfully synthesized, and both incorporated the new generation Ir(III) anticancer complex $[(\eta^5\text{-Cp}^{\text{xbiph}})\text{Ir(phpy)(py)}]\text{PF}_6$ into self-assembled nanoparticles. Although these nanoparticles gave rise to the tumor-targeted delivery of the Ir anticancer drug, HA-ss-Py micelles released it more rapidly than the HA-Py micelles under acidic and reducing environment. The present cell-based studies showed enhanced intracellular uptake of both HA-ss-Py and HA-Py nanoparticles through HA receptor-mediated endocytosis, specifically via interactions with CD44 receptors on tumor cells. Moreover, our *in vivo* studies demonstrated a high tumor-targeting and therapeutic efficacy of HA-ss-Py-Ir and HA-Py-Ir nanoparticles as compared to the free Ir anticancer drug. These data confirm the EPR effect of these nanoparticles, reflecting the HA receptor-mediated endocytosis and pH and reduction-responsive drug release. The present multifunctional pH- and reduction-

responsive drug delivery system has a potential as a highly efficient Ir(III) anticancer drug delivery vehicle for targeted cancer therapy.

Acknowledgements

This work was supported by the National Natural Science Foundation of China (Grant No. 21074071).

Abbreviations

HA, hyaluronan or hyaluronic acid; M_w, molecular weight; Ir(III), organoiridium(III) complex; Py, Pyrene; HA-ss-Py, HA-cystamin-pyrenyl; HA-Py, HA-pyrenyl; HA-ss-Py-Ir, HA-cystamin-pyrenyl-iridium; HA-Py-Ir, HA-pyrenyl-iridium; DLS, dynamic light scattering; GSH, glutathione; EPR, enhanced permeability and retention; EDC, 1-ethyl-3-(3-dimethylaminopropyl) carbodiimide; NHS, N-hydroxysuccinimide; MTT, 3-(4,5-dimethyl-thiazol-2-yl)-2,5-diphenyl tetrazolium bromide; PBS, phosphate-buffered saline; HOBt, 1-Hydroxybenzotriazole; CMC, critical micelle concentrations; CLSM, confocal laser scanning microcopy.

REFERENCES

1. Wong, E.; Giandomenico, C. M., Current status of platinum-based antitumor drugs. *Chemical Reviews* **1999,** 99, (9), 2451-2466.

2. Cohen, S. M.; Lippard, S. J., Cisplatin: From DNA damage to cancer chemotherapy. *Progress in Nucleic Acid Research and Molecular Biology* **2001,** 67, 93-130.

3. Stewart, D. J., Mechanisms of resistance to cisplatin and carboplatin. *Critical Reviews in Oncology/Hematology* **2007,** 63, (1), 12-31.

4. Kelland, L., The resurgence of platinum-based cancer chemotherapy. *Nat Rev Cancer* **2007,** 7, (8), 573-584.

5. Gasser, G.; Ott, I.; Metzler-Nolte, N., Organometallic Anticancer Compounds. *J Med Chem* **2011,** 54, (1), 3-25.

6. Suss-Fink, G., Arene ruthenium complexes as anticancer agents. *Dalton T* **2010,** 39, (7), 1673-1688.

7. Ma, D. L.; Liu, L. J.; Leung, K. H.; Chen, Y. T.; Zhong, H. J.; Chan, D. S. H.; Wang, H. M. D.; Leung, C. H., Antagonizing STAT3 Dimerization with a Rhodium(III) Complex. *Angew Chem Int Edit* **2014,** 53, (35), 9178-9182.

8. Bruijnincx, P. C. A.; Sadler, P. J., Controlling platinum, ruthenium, and osmium reactivity for anticancer drug design. In *Advances in Inorganic Chemistry*, Rudi van, E.; Colin, D. H., Eds. Elsevier Academic Press: San Diego, CA, 2009; Vol. 61, pp 1-62.

9. Liu, Z.; Sadler, P. J., Organoiridium Complexes: Anticancer Agents and Catalysts. *Accounts Chem Res* **2014,** 47, (4), 1174-1185.

10. Hearn, J. M.; Romero-Canelon, I.; Qamar, B.; Liu, Z.; Hands-Portman, I.; Sadler, P. J., Organometallic Iridium(III) Anticancer Complexes with New Mechanisms of Action: NCI-60 Screening, Mitochondrial Targeting, and Apoptosis. *Acs Chem Biol* **2013,** 8, (6), 1335-1343.

11. Liu, Z.; Habtemariam, A.; Pizarro, A. M.; Clarkson, G. J.; Sadler, P. J., Organometallic Iridium(III) Cyclopentadienyl Anticancer Complexes Containing C,N-Chelating Ligands. *Organometallics* **2011,** 30, (17), 4702-4710.

12. Liu, Z.; Romero-Canelon, I.; Habtemariam, A.; Clarkson, G. J.; Sadler, P. J., Potent Half-Sandwich Iridium(III) Anticancer Complexes Containing C boolean AND I-Chelated and Pyridine Ligands. *Organometallics* **2014,** 33, (19), 5324-5333.

13. Liu, Z.; Romero-Canelon, I.; Qamar, B.; Hearn, J. M.; Habtemariam, A.; Barry, N. P. E.; Pizarro, A. M.; Clarkson, G. J.; Sadler, P. J., The Potent Oxidant Anticancer Activity of Organoiridium Catalysts. *Angew Chem Int Edit* **2014,** 53, (15), 3941-3946.

14. Millett, A. J.; Habtemariam, A.; Romero-Canelon, I.; Clarkson, G. J.; Sadler, P. J., Contrasting Anticancer Activity of Half-Sandwich Iridium(III) Complexes Bearing Functionally Diverse 2-Phenylpyridine Ligands. *Organometallics* **2015,** 34, (11), 2683-2694.

15. Hartinger, C. G.; Metzler-Nolte, N.; Dyson, P. J., Challenges and Opportunities in the Development of Organometallic Anticancer Drugs. *Organometallics* **2012,** 31, (16), 5677-5685.

16. Starha, P.; Habtemariam, A.; Romero-Canelon, I.; Clarkson, G. J.; Sadler, P. J., Hydrosulfide Adducts of Organo-Iridium Anticancer Complexes. *Inorg Chem* **2016,** 55, (5), 2324-2331.

17. Riehemann, K.; Schneider, S. W.; Luger, T. A.; Godin, B.; Ferrari, M.; Fuchs, H., Nanomedicine-Challenge and Perspectives. *Angew Chem Int Edit* **2009,** 48, (5), 872-897.

18. Yang, X. Y.; Du, H. L.; Liu, J. Y.; Zhai, G. X., Advanced Nanocarriers Based on Heparin and Its Derivatives for Cancer Management. *Biomacromolecules* **2015,** 16, (2), 423-436.

19. Huang, P.; Wang, D. L.; Su, Y.; Huang, W.; Zhou, Y. F.; Cui, D. X.; Zhu, X. Y.; Yan, D. Y., Combination of Small Molecule Prodrug and Nanodrug Delivery: Amphiphilic Drug-Drug Conjugate for Cancer Therapy. *J Am Chem Soc* **2014,** 136, (33), 11748-11756.

20. Lee, S.-M.; Chen, H.; Dettmer, C. M.; O'Halloran, T. V.; Nguyen, S. T., Polymer-Caged Lipsomes: A pH-Responsive Delivery System with High Stability. *J Am Chem Soc* **2007,** 129, (49), 15096-15097.

21. Al-Jamal, W. T.; Kostarelos, K., Liposomes: From a Clinically Established Drug Delivery System to a Nanoparticle Platform for Theranostic Nanomedicine. *Accounts Chem Res* **2011,** 44, (10), 1094-1104.

22. Linderoth, L.; Fristrup, P.; Hansen, M.; Melander, F.; Madsen, R.; Andresen, T. L.; Peters, G. H., Mechanistic Study of the sPLA2-Mediated Hydrolysis of a Thio-ester Pro Anticancer Ether Lipid. *J Am Chem Soc* **2009,** 131, (34), 12193-12200.

23. Dhar, S.; Liu, Z.; Thomale, J.; Dai, H. J.; Lippard, S. J., Targeted single-wall carbon nanotube-mediated Pt(IV) prodrug delivery using folate as a homing device. *J Am Chem Soc* **2008,** 130, (34), 11467-11476.

24. Liu, Z.; Robinson, J. T.; Sun, X. M.; Dai, H. J., PEGylated nanographene oxide for delivery of water-insoluble cancer drugs. *J Am Chem Soc* **2008,** 130, (33), 10876-10877.

25. Ambrogio, M. W.; Thomas, C. R.; Zhao, Y.-L.; Zink, J. I.; Stoddart, J. F., Mechanized Silica Nanoparticles: A New Frontier in Theranostic Nanomedicine. *Accounts Chem Res* **2011,** 44, (10), 903-913.

26. Vallet-Regi, M.; Colilla, M.; Gonzalez, B., Medical applications of organic-inorganic hybrid materials within the field of silica-based bioceramics. *Chem Soc Rev* **2011,** 40, (2), 596-607.

27. Du, J. Z.; Sun, T. M.; Song, W. J.; Wu, J.; Wang, J., A Tumor-Acidity-Activated Charge-Conversional Nanogel as an Intelligent Vehicle for Promoted Tumoral-Cell Uptake and Drug Delivery. *Angew Chem Int Edit* **2010,** 49, (21), 3621-3626.

28. Kim, E.; Kim, D.; Jung, H.; Lee, J.; Paul, S.; Selvapalam, N.; Yang, Y.; Lim, N.; Park, C. G.; Kim, K., Facile, Template-Free Synthesis of Stimuli-Responsive Polymer Nanocapsules for Targeted Drug Delivery. *Angew Chem Int Edit* **2010,** 49, (26), 4405-4408.

29. Saravanakumar, G.; Min, K. H.; Min, D. S.; Kim, A. Y.; Lee, C.-M.; Cho, Y. W.; Lee, S. C.; Kim, K.; Jeong, S. Y.; Park, K.; Park, J. H.; Kwon, I. C., Hydrotropic oligomer-conjugated glycol chitosan as a carrier of paclitaxel: Synthesis, characterization, and in vivo biodistribution. *J Control Release* **2009,** 140, (3), 210-217.

30. Nicolas, J.; Mura, S.; Brambilla, D.; Mackiewicz, N.; Couvreur, P., Design, functionalization strategies and biomedical applications of targeted biodegradable/biocompatible polymer-based nanocarriers for drug delivery. *Chem Soc Rev* **2013,** 42, (3), 1147-1235.

31. Farokhzad, O. C.; Langer, R., Impact of Nanotechnology on Drug Delivery. *Acs Nano* **2009,** 3, (1), 16-20.

32. Duncan, R., The dawning era of polymer therapeutics. *Nature Reviews Drug Discovery* **2003,** 2, (5), 347-360.

33. Ferrari, M., Cancer nanotechnology: opportunities and challenges. *Nat Rev Cancer* **2005,** 5, (3), 161-171.

34. Sun, W.; Li, S.; Haupler, B.; Liu, J.; Jin, S.; Steffen, W.; Schubert, U. S.; Butt, H. J.; Liang, X. J.; Wu, S., An Amphiphilic Ruthenium Polymetallodrug for Combined Photodynamic Therapy and Photochemotherapy In Vivo. *Adv Mater* **2017,** 29, (6).

35. Chen, W.; Zou, Y.; Jia, J. N.; Meng, F. H.; Cheng, R.; Deng, C.; Feijen, J.; Zhong, Z. Y., Functional Poly(epsilon-caprolactone)s via Copolymerization of epsilon-Caprolactone and Pyridyl Disulfide-Containing Cyclic Carbonate: Controlled Synthesis and Facile Access to Reduction-Sensitive Biodegradable Graft Copolymer Micelles. *Macromolecules* **2013,** 46, (3), 699-707.

36. Yen, H. C.; Cabral, H.; Mi, P.; Toh, K.; Matsumoto, Y.; Liu, X.; Koori, H.; Kim, A.; Miyazaki, K.; Miura, Y.; Nishiyama, N.; Kataoka, K., Light-Induced Cytosolic Activation of

Reduction-Sensitive Camptothecin-Loaded Polymeric Micelles for Spatiotemporally Controlled in Vivo Chemotherapy. *Acs Nano* **2014,** 8, (11), 11591-11602.

37. Liu, Z.; Jiao, Y.; Wang, Y.; Zhou, C.; Zhang, Z., Polysaccharides-based nanoparticles as drug delivery systems. *Adv Drug Deliver Rev* **2008,** 60, (15), 1650-1662.

38. Chen, H. T.; Kim, S. W.; Li, L.; Wang, S. Y.; Park, K.; Cheng, J. X., Release of hydrophobic molecules from polymer micelles into cell membranes revealed by Forster resonance energy transfer imaging. *P Natl Acad Sci USA* **2008,** 105, (18), 6596-6601.

39. Shamay, Y.; Adar, L.; Ashkenasy, G.; David, A., Light induced drug delivery into cancer cells. *Biomaterials* **2011,** 32, (5), 1377-1386.

40. Li, J.; Huo, M. R.; Wang, J.; Zhou, J. P.; Mohammad, J. M.; Zhang, Y. L.; Zhu, Q. N.; Waddad, A. Y.; Zhang, Q., Redox-sensitive micelles self-assembled from amphiphilic hyaluronic acid-deoxycholic acid conjugates for targeted intracellular delivery of paclitaxel. *Biomaterials* **2012,** 33, (7), 2310-2320.

41. Yang, X. Z.; Du, J. Z.; Dou, S.; Mao, C. Q.; Long, H. Y.; Wang, J., Sheddable Ternary Nanoparticles for Tumor Acidity-Targeted siRNA Delivery. *Acs Nano* **2012,** 6, (1), 771-781.

42. Azagarsamy, M. A.; Sokkalingam, P.; Thayumanavan, S., Enzyme-Triggered Disassembly of Dendrimer-Based Amphiphilic Nanocontainers. *J Am Chem Soc* **2009,** 131, (40), 14184-14185.

43. Chen, W.; Zhong, P.; Meng, F. H.; Cheng, R.; Deng, C.; Feijen, J.; Zhong, Z. Y., Redox and pH-responsive degradable micelles for dually activated intracellular anticancer drug release. *J Control Release* **2013,** 169, (3), 171-179.

44. Liu, C. Y.; Yuan, J.; Luo, X. M.; Chen, M. H.; Chen, Z. J.; Zhao, Y. C.; Li, X. H., Folate-Decorated and Reduction-Sensitive Micelles Assembled from Amphiphilic Polymer-

Camptothecin Conjugates for Intracellular Drug Delivery. *Mol Pharmaceut* **2014,** 11, (11), 4258-4269.

45. Meng, F.; Hennink, W. E.; Zhong, Z., Reduction-sensitive polymers and bioconjugates for biomedical applications. *Biomaterials* **2009,** 30, (12), 2180-2198.

46. Cheng, R.; Feng, F.; Meng, F.; Deng, C.; Feijen, J.; Zhong, Z., Glutathione-responsive nano-vehicles as a promising platform for targeted intracellular drug and gene delivery. *J Control Release* **2011,** 152, (1), 2-12.

47. Lee, E. S.; Gao, Z. G.; Bae, Y. H., Recent progress in tumor pH targeting nanotechnology. *J Control Release* **2008,** 132, (3), 164-170.

48. Gao, W. W.; Chan, J. M.; Farokhzad, O. C., pH-Responsive Nanoparticles for Drug Delivery. *Mol Pharmaceut* **2010,** 7, (6), 1913-1920.

49. Chen, J.; Qiu, X. Z.; Ouyang, J.; Kong, J. M.; Zhong, W.; Xing, M. M. Q., pH and Reduction Dual-Sensitive Copolymeric Micelles for Intracellular Doxorubicin Delivery. *Biomacromolecules* **2011,** 12, (10), 3601-3611.

50. Li, M. Q.; Tang, Z. H.; Sun, H.; Ding, J. X.; Song, W. T.; Chen, X. S., pH and reduction dual-responsive nanogel cross-linked by quaternization reaction for enhanced cellular internalization and intracellular drug delivery. *Polym Chem-Uk* **2013,** 4, (4), 1199-1207.

51. Pan, Y. J.; Chen, Y. Y.; Wang, D. R.; Wei, C.; Guo, J.; Lu, D. R.; Chu, C. C.; Wang, C. C., Redox/pH dual stimuli-responsive biodegradable nanohydrogels with varying responses to dithiothreitol and glutathione for controlled drug release. *Biomaterials* **2012,** 33, (27), 6570-6579.

52. Wu, L. L.; Zou, Y.; Deng, C.; Cheng, R.; Meng, F. H.; Zhong, Z. Y., Intracellular release of doxorubicin from core-crosslinked polypeptide micelles triggered by both pH and reduction conditions. *Biomaterials* **2013,** 34, (21), 5262-5272.

53. Toole, B. P., Hyaluronan: from extracellular glue to pericellular cue. *Nat Rev Cancer* **2004,** 4, (7), 528-539.

54. Lapčík, L.; Lapčík, L.; De Smedt, S.; Demeester, J.; Chabreček, P., Hyaluronan: Preparation, Structure, Properties, and Applications. *Chemical Reviews* **1998,** 98, (8), 2663-2684.

55. Morra, M., Engineering of biomaterials surfaces by hyaluronan. *Biomacromolecules* **2005,** 6, (3), 1205-1223.

56. Kogan, G.; Soltes, L.; Stern, R.; Gemeiner, P., Hyaluronic acid: a natural biopolymer with a broad range of biomedical and industrial applications. *Biotechnol Lett* **2007,** 29, (1), 17-25.

57. Zhang, F.; Wu, J.; Kang, D.; Zhang, H. B., Development of a complex hydrogel of hyaluronan and PVA embedded with silver nanoparticles and its facile studies on Escherichia coli. *J Biomat Sci-Polym E* **2013,** 24, (12), 1410-1425.

58. Götte, M.; Yip, G. W., Heparanase, Hyaluronan, and CD44 in Cancers: A Breast Carcinoma Perspective. *Cancer Research* **2006,** 66, (21), 10233-10237.

59. Platt, V. M.; Szoka, F. C., Anticancer therapeutics: Targeting macromolecules and nanocarriers to hyaluronan or CD44, a hyaluronan receptor. *Mol Pharmaceut* **2008,** 5, (4), 474-486.

60. Han, H. S.; Thambi, T.; Choi, K. Y.; Son, S.; Ko, H.; Lee, M. C.; Jo, D. G.; Chae, Y. S.; Kang, Y. M.; Lee, J. Y.; Park, J. H., Bioreducible Shell-Cross-Linked Hyaluronic Acid Nanoparticles for Tumor-Targeted Drug Delivery. *Biomacromolecules* **2015,** 16, (2), 447-456.

61. Wang, L.; Wang, Y.; Jin, Q.; Jia, F.; Wang, H. B.; Ji, J., Biomimic pH/reduction dual-sensitive reversibly cross-linked hyaluronic acid prodrug micelles for targeted intracellular drug delivery. *Polymer* **2015,** 76, 237-244.

62. Dosio, F.; Arpicco, S.; Stella, B.; Fattal, E., Hyaluronic acid for anticancer drug and nucleic acid delivery. *Adv Drug Deliver Rev* **2016,** 97, 204-236.

63. Wang, X.; Li, Y.; Li, Q.; Neufeld, C. I.; Pouli, D.; Sun, S.; Yang, L.; Deng, P.; Wang, M.; Georgakoudi, I.; Tang, S.; Xu, Q., Hyaluronic acid modification of RNase A and its intracellular delivery using lipid-like nanoparticles. *J Control Release* **2017,** DOI: 10.1016/j.jconrel.2017.01.037.

64. Cai, Z.; Zhang, H.; Wei, Y.; Cong, F., Hyaluronan-inorganic nanohybrid materials for biomedical applications. *Biomacromolecules* **2017,** DOI: 10.1021/acs.biomac.7b00424.

65. Liu, Z.; Habtemariam, A.; Pizarro, A. M.; Fletcher, S. A.; Kisova, A.; Vrana, O.; Salassa, L.; Bruijnincx, P. C. A.; Clarkson, G. J.; Brabec, V.; Sadler, P. J., Organometallic Half-Sandwich Iridium Anticancer Complexes. *J Med Chem* **2011,** 54, (8), 3011-3026.

66. Grishagin, I. V.; Pollock, J. B.; Kushal, S.; Cook, T. R.; Stang, P. J.; Olenyuk, B. Z., In vivo anticancer activity of rhomboidal Pt(II) metallacycles. *Proc Natl Acad Sci U S A* **2014,** 111, (52), 18448-53.

67. Dubikovskaya, E. A.; Thorne, S. H.; Pillow, T. H.; Contag, C. H.; Wender, P. A., Overcoming multidrug resistance of small-molecule therapeutics through conjugation with releasable octaarginine transporters. *P Natl Acad Sci USA* **2008,** 105, (34), 12128-12133.

68. Hu, F. Q.; Liu, L. N.; Du, Y. Z.; Yuan, H., Synthesis and antitumor activity of doxorubicin conjugated stearic acid-g-chitosan oligosaccharide polymeric micelles. *Biomaterials* **2009,** 30, (36), 6955-6963.

69. Balendiran, G. K.; Dabur, R.; Fraser, D., The role of glutathione in cancer. *Cell Biochem Funct* **2004,** 22, (6), 343-352.

70. Yin, S. P.; Huai, J.; Chen, X.; Yang, Y.; Zhang, X. X.; Gan, Y.; Wang, G. J.; Gu, X. C.; Li, J., Intracellular delivery and antitumor effects of a redox-responsive polymeric paclitaxel conjugate based on hyaluronic acid. *Acta Biomater* **2015,** 26, 274-285.

71. Koo, A. N.; Min, K. H.; Lee, H. J.; Lee, S.-U.; Kim, K.; Chan Kwon, I.; Cho, S. H.; Jeong, S. Y.; Lee, S. C., Tumor accumulation and antitumor efficacy of docetaxel-loaded core-shell-corona micelles with shell-specific redox-responsive cross-links. *Biomaterials* **2012,** 33, (5), 1489-1499.

72. Tokita, Y.; Okamoto, A., Hydrolytic degradation of hyaluronic acid. *Polymer Degradation and Stability* **1995,** 48, (2), 269-273.

73. Penno, M. B.; August, J. T.; Baylin, S. B.; Mabry, M.; Linnoila, R. I.; Lee, V. S.; Croteau, D.; Yang, X. L.; Rosada, C., Expression of CD44 in Human Lung Tumors. *Cancer Research* **1994,** 54, (5), 1381-1387.

74. Datir, S. R.; Das, M.; Singh, R. P.; Jain, S., Hyaluronate Tethered, "Smart" Multiwalled Carbon Nanotubes for Tumor-Targeted Delivery of Doxorubicin. *Bioconjugate Chem* **2012,** 23, (11), 2201-2213.

75. Greenspan, P.; Mayer, E. P.; Fowler, S. D., Nile red: a selective fluorescent stain for intracellular lipid droplets. *The Journal of Cell Biology* **1985,** 100, (3), 965-973.

76. Jiang, W.; Kim, B. Y. S.; Rutka, J. T.; Chan, W. C. W., Nanoparticle-mediated cellular response is size-dependent. *Nat Nanotechnol* **2008,** 3, (3), 145-150.

77. Zhang, S. L.; Li, J.; Lykotrafitis, G.; Bao, G.; Suresh, S., Size-Dependent Endocytosis of Nanoparticles. *Adv Mater* **2009,** 21, (4), 419-424.

78. Lin, C. J.; Kuan, C. H.; Wang, L. W.; Wu, H. C.; Chen, Y. C.; Chang, C. W.; Huang, R. Y.; Wang, T. W., Integrated self-assembling drug delivery system possessing dual responsive and active targeting for orthotopic ovarian cancer theranostics. *Biomaterials* **2016,** 90, 12-26.

79. Wang, R.; Luo, Y.; Yang, S.; Lin, J.; Gao, D.; Zhao, Y.; Liu, J.; Shi, X.; Wang, X., Hyaluronic acid-modified manganese-chelated dendrimer-entrapped gold nanoparticles for the targeted CT/MR dual-mode imaging of hepatocellular carcinoma. *Scientific Reports* **2016,** 6, 33844.

80. Liang, J. M.; Zeng, F.; Zhang, M.; Pan, Z. Z.; Chen, Y. Z.; Zeng, Y. N.; Xu, Y.; Xu, Q.; Huang, Y. Z., Green synthesis of hyaluronic acid-based silver nanoparticles and their enhanced delivery to CD44(+) cancer cells. *Rsc Adv* **2015,** 5, (54), 43733-43740.

81. Jaracz, S.; Chen, J.; Kuznetsova, L. V.; Ojima, I., Recent advances in tumor-targeting anticancer drug conjugates. *Bioorganic & Medicinal Chemistry* **2005,** 13, (17), 5043-5054.

TOC

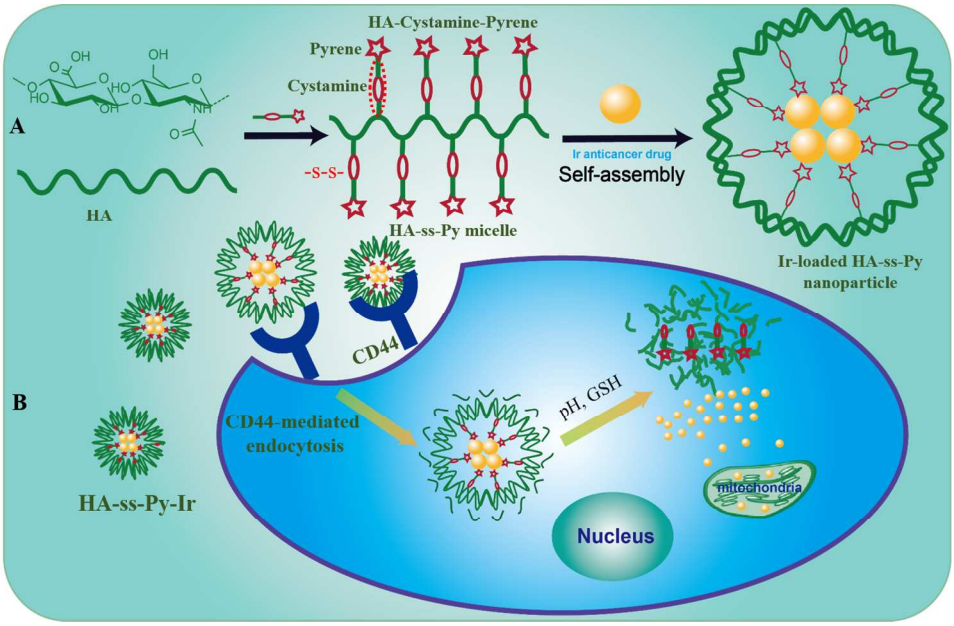
HA-Cystamine-Pyrene
Pyrene
Cystamine
-S-S-
A
HA
HA-ss-Py micelle
Ir anticancer drug
Self-assembly
Ir-loaded HA-ss-Py nanoparticle
CD44
B
CD44-mediated endocytosis
pH, GSH
HA-ss-Py-Ir
mitochondria
Nucleus